

Project Numbers: MQP-BIO-JXR-2005
MQP-BME-JXR-2005

Osteogenic potential of silk scaffold functionalized with growth factors

A Major Qualifying Project Report:

Submitted to the Faculty of the

WORCESTER POLYTECHNIC INSTITUTE

in partial fulfillment of the requirements for the

Degree of Bachelor of Science

by

Kristen Kane

Beth Lorusso

April 28, 2005

Approved:

Professor Jill Rulfs

Professor Satya Shivkumar

Abstract

There is renewed interest in silks as a biomaterial due to their unique mechanical properties, highly organized structure, and diverse surface chemistry. This study investigates silk's efficacy as an alternative biomaterial for bone regeneration and analyzes the role of adhesion and signaling factors in the process. Femoral defects in rodents were implanted with a series of scaffold combinations. Parameters included scaffold decoration (RGD or BMP-2) and hMSCs. Radiological and DEXA analyses demonstrated that scaffolds with BMP-2 and empty scaffolds produced the most bone ingrowth and defect bridging.

Table of Contents

Abstract	1
Table of Figures	3
Table of Tables	4
Authorship	5
Acknowledgments	6
I. Introduction	7
II. Literature Review	10
1. <i>Bone Tissue Engineering</i>	10
2. <i>Bone Scaffold Requirements</i>	12
3. <i>Synthetic Bone Graft Substitutes</i>	15
4. <i>Natural Bone Graft Substitutes</i>	19
6. <i>Silk Scaffold for Bone Formation</i>	22
III. Objectives	40
IV. Materials and Methods	41
7. <i>Materials</i>	41
8. <i>Silk Preparation</i>	41
9. <i>Silk Scaffold Fabrication</i>	44
10. <i>Modification of Silk by Covalent Coupling of Peptides</i>	45
11. <i>Human Mesenchymal Stem Cell Isolation and Expansion</i>	48
12. <i>Operative Procedure</i>	48
12.1 <i>Femoral Segmental Defect</i>	48
12.2 <i>Post-Operative Procedure</i>	51
13. <i>Scanning Electron Microscopy (SEM)</i>	53
14. <i>Radiographs</i>	53
15. <i>Dual Energy X-ray Absorptiometry (DEXA) Scanning</i>	54
V. Experimental Design	56
16. <i>Matrix Preparation</i>	56
17. <i>Characterization of Matrix</i>	60
18. <i>Peptide Coupling</i>	61
19. <i>Model System</i>	63
20. <i>Assessment of in vivo Bone Formation</i>	65
VI. Results	66
21. <i>X-ray Evaluation</i>	66
22. <i>DEXA scanning</i>	70
VII. Discussion	75
VIII. Conclusions	82
IX. Future Recommendations	83
References	85
Appendices	89

Table of Figures

Figure 1: Stress-strain curve of trabecular bone	13
Figure 2: Organization of hydrophilic and hydrophobic domains in silk proteins.....	23
Figure 3: Schematic organization of crystalline and amorphous regions in a silk fiber	26
Figure 4: Stress-strain curves of (a) native <i>B. mori</i> silk fibroin fiber and (b)-(e) regenerated <i>B. mori</i> fibroin fibers.....	32
Figure 5: Methodology for Silk Scaffold Preparation	43
Figure 6: Silk scaffold fabrication flowchart with HFIP-derived silk	44
Figure 7: Process by which the silk was modified by covalent couplings of RGD peptides.....	47
Figure 8: Surgical procedure for placing silk scaffolds in critical size femoral defects.....	50
Figure 9: Critical size femoral defect fixed externally with a plate	51
Figure 10: SEM images of the inner and outer structure of the silk scaffold by salt leaching and gas foaming after methanol treatment	57
Figure 11: Adhesion of bovine mesenchymal stem cell fibroblasts to silk substrates	62
Figure 12: (A) Nodule numbers and (B) areas formed by the Saos-2 osteoblast-like, human osteoblasts	63
Figure 13: Qualitative analyses for bridging of the defect and percentage of bone ingrowth.	67
Figure 14: X-rays that were taken of the femoral defect	69
Figure 15: DEXA scanning of femoral defect with implants for mineral density (g/cm^2), area (cm^2), and bone content (g).....	70
Figure 16: The average DEXA values (Regions 1-3) compared to control values of the healthy, opposite hind limb of the rodents.....	73
Figure 17: SEM of hMSCs in HFIP silk scaffolds	74
Figure 18: Qualitative analyses for bridging of the defect and percentage of bone ingrowth from previous experiment	77
Figure 19: DEXA scanning of femoral defect with implants for new bone area (cm^2) (black columns), mineral density (g/cm^2) (white columns) and content (g) (gray columns) from previous experiment	78

Table of Tables

Table 1: Mechanical Properties of Bone Compared to Bone Replacement Structures	13
Table 2: Bone Replacement Materials	15
Table 3: Properties of Selected Synthetic Biodegradable Polymers.....	17
Table 4: Mechanical Properties of Select Biodegradable Polymers.....	18
Table 5: Comparison of Bone Graft Materials	20
Table 6: Mechanical Properties of common bone replacement structures	21
Table 7: Summary of Components of Hydrophilic and Hydrophobic Components of fibroin Sequences.....	24
Table 8: Amino acid composition of silk fibroin and one glue protein (mol%) from four different species	27
Table 9: List of Lepidoptera, Diptera, and spider species and their silk producing gland	28
Table 10: Comparison of extensibility, elastic modulus, and tensile strength of silks.....	29
Table 11: Mechanical properties of silkworm and dragline silk compared to other materials	31
Table 12: Scaffold Groups	51
Table 13: Qualitative X-ray Measurements	54
Table 14: Porosity and Density of the Scaffolds (Average \pm S.D., N=3) for Porosity and Density Measures (for Pore Sizes, N= 200)	57
Table 15: Compressive Stress and Modulus of the Silk Scaffolds.....	58
Table 16: Average Compressive Strength and Average Compressive Modulus of Gas Foamed and Salt Leached Scaffold at 1% and 2% Strain under Compressive Load	58
Table 17: Treatment groups for previous group of rats studied for critical size femoral defects	76

Authorship

1. Abstract: Beth and Kristen
2. Introduction: Kristen
3. Literature Review: Beth and Kristen
4. Objectives: Beth and Kristen
5. Experimental Design: Beth and Kristen
6. Results: Beth and Kristen
7. Discussion: Beth and Kristen
8. Conclusions: Beth and Kristen
9. Future Recommendations: Beth

Acknowledgments

In the completion of this Major Qualifying Project, we would like to thank our advisors Professor Jill Rulfs and Professor Satya Shivkumar for their guidance. Additionally, we would like to thank Dr. Carl Kirker-Head and Dr. David Kaplan of Tufts University for their valuable knowledge and assistance in the areas of orthopedics, *in vivo* studies, and tissue engineering. We would also like to thank Hyeon Joo Kim and Lauren Abrahamsen for their help throughout our project.

I. Introduction

In 1988 there were more than 3 million musculoskeletal surgeries performed world wide and more than 450,000 in United States alone (Laurencin *et al.*, 1999). Bone that has been damaged from degenerative disease and large bone tumors, and from massive fractures, defects and non-unions have presented major challenges to reconstructive surgery. Most procedures rely on the traditional therapies of bone grafting, although there are other techniques currently being explored. Orthopedic surgeons perform over 800,000 bone graft procedures annually, which require donor tissue obtained from either the patient or another person and implanted at the injury site (Laurencin *et al.*, 1999). While these treatments have proved fairly successful, there are several drawbacks associated with its use. A second surgical site is required, there is a possibility of rejection, and the graft supply may be insufficient.

The problems associated with bone grafting have caused new treatments to emerge with promise to circumvent the limitations. Scientists have begun to look at tissue engineering to restore tissue function by regenerating or growing bone. Bone tissue engineering approaches include the use of a 3-dimensional, porous, degradable matrix. Another approach extracts the patient's own bone-making cells which are grown in culture. Both of the matrices can be transplanted back into the patient. In order to accomplish this objective, a unique set of environmental conditions must be met. These conditions include: an appropriate blood supply which provides access for bone making cells and nutrients and eliminates wastes; and a scaffold which serves as a template for new bone to be formed very similar to that during growth. Therefore, the scaffold design must meet specific requirements for bone formation.

Previous studies of bone formation have included scaffold materials such as synthetic and natural polymers, ceramics, and composites. However, the types of materials available today

remain limited. In order to highlight the relative merits of silk-based scaffolds for bone formation, comparisons will be made to some of the most commonly used biomaterials for scaffolds today. Collagens have fewer options for engineering control of its structure and thus mechanical properties due to the primary sequence containing essentially one repetitive block (Gly-Pro-HyP). Generally, comparisons to synthetic polymers, such as families of polyesters, have limited control of properties and chemical diversity mainly due to the presence of only one or two monomers in the chain (in comparison to the 20 or so present in silk proteins). Calcium phosphates have been used due to their similarity to the mineral component of bone. However, the success has been limited because the biomaterial as a scaffold lacks bioactive behavior (being integrated into the tissue by the same processes present in modeling native bone). This limitation is due to its stability and hence extremely slow degradation rate. The rates of degradation for silk have the ability to be closely regulated through control of primary sequences and crystallinity. Matching the unique mechanical properties of native bone remains a challenge with many current biomaterials.

It should be recognized that the principal scaffolds explored to date for bone replacement or regeneration have shown promise, some even approved by the U.S. Food and Drug Administration (FDA). However, the shortcomings associated with these biomaterials have prompted the need to identify alternate scaffolds to overcome these limitations. Presently, there is no bone substitute that functionally and mechanically mimics natural autogenous bone.

The principal goal of this project is to investigate the use of silk fibroin as an alternative scaffold material for the facilitation of bone regeneration. Silks offer remarkable mechanical properties with a very high strength and resistance to compression, are readily accepted by the body (biocompatible), and have a diverse range of surface chemistries for selective chemical

couplings (Sofia *et al.*, 2000). Additionally, the interactions between cell signaling factors, human mesenchymal stem cells, and the silk proteins in relation to bone formation are explored. Specific peptides related to cell adhesion (RGD) and bone formation (BMP-2) will be chemically functionalized to the silk proteins in combinations with or without stem cells to develop a clearer understanding of the relationships between decoration type and cell responses.

II. Literature Review

Traditional surgical methods and current scaffold biomaterials have not yet proved ideal for bone regeneration. Cell-based therapies have been utilized to improve the regeneration of the damaged osseous region. The scaffold used is an essential component in tissue engineering and must meet certain compositional, architectural, and physiochemical requirements in order to mimic that of natural bone and influence appropriate tissue formation. Most scaffolds used today meet only few criteria for bone repair and therefore silk is explored as a biomaterial particularly due to their inherent mechanical properties.

1. *Bone Tissue Engineering*

Surgical treatments such as allografts and autografts have been used to repair bone defects. Autografts, which are transplants from the patient's own bone, are considered the gold standard because they are able to regenerate bone without any immunological affect. They also provide osteoinductive and osteoconductive properties, and are usually well incorporated into the graft site (Arrington *et al.*, 1996). However, a second surgical site is required which leads to added discomfort and an extended recovery period. Additionally, obtaining a sufficient amount of bone from the patient can not only be difficult, but it can also be extremely painful.

Allografts, on the other hand, utilize bone from others' for bone repair. With this technique, bone repair capability is not as successful. It is more expensive, increases donor site morbidity compared with autografts, and can be detrimental to the recipient if the transplant carries a disease or causes an immunological reaction (Petite, 2000). Allogenic bone maintains osteoconductive properties but loses osteoinductive potential as a result of processing and radiation. Although these methods have been widely used by doctors and have proved fairly

successful, their shortcomings have prompted the medical world to look to tissue engineering and a variety of biologic and synthetic scaffolds to facilitate bone formation.

This area of research has the capacity to repair or restore living tissue by using biomaterials, stem cells, and growth factors alone or in combination. Therapies in bone tissue engineering include cell, gene, or cytokine therapy (Saito *et al.*, 2003). In gene therapy, the gene that produces a particular protein is directly transferred to the cells *in vivo* or *in vitro*. The gene then releases the desired protein into the injured area. This method is beneficial because it allows for a sustained local release of the protein which would provide a longer stimulus, maintaining the signals to create new bone (Saito *et al.*, 2003). Studies have aimed to modify fibroblast cells in bone to generate bone morphogenetic protein-2 (BMP-2) or parathyroid hormone (PTH1-34) (Fang *et al.*, 1996).

Cell-based strategies have been researched for bone regeneration in which cells with osteogenic potential, derived from the bone marrow, are transplanted directly into the defect and differentiate into the desired lineage. Also the incorporation of proteins or genetically engineered cells can be transplanted to promote regeneration through induction of osteoblast differentiation (Saito *et al.*, 2003). With this comes the need to develop matrices that will support the cell attachment, proliferation, differentiation, as well as deliver the bioactive factors and/or host cells (Saito *et al.*, 2003).

The scaffold design is essential in tissue engineering. The composition, architecture, and physiochemical properties play a prominent role in the capability of new bone tissue to form. The minimal requirements that a scaffolds should meet are discussed in the next section.

2. Bone Scaffold Requirements

In order to meet the challenging biological, mechanical, and degradation features of bone repair and regeneration, there are several requirements that scaffolds must possess. Important biological requirements are that the scaffold should not produce an inflammatory, immunogenic, or cytotoxic response *in vivo* (biocompatible). The construct should also resorb in a controlled manner consistent with the rate of new bone ingrowth and release nontoxic by-products following degradation (Yaszemski *et al.*, 1996). The degradation products should be biocompatible and readily metabolized or removed from the body. In addition to these requirements, the material must be osteoinductive, inducing differentiation into osteogenic cells.

Mechanical performance of a scaffold is an imperative and difficult feature to mimic due to the complex nature of bone. The skeleton has numerous functions, but one important function is its ability to bear load. The mechanical properties of bone are unique in that they have high compressive and tensile strength. However, bone is capable of withstanding higher compressive strengths before fracture compared to tensile strength. The mechanical properties are attributed to its composition; a type I collagen extracellular matrix and other organic materials give tensile strength, while hydroxyapatite is responsible for resistance to compression. Around 30% of bone is composed of the organic compound collagen (90 - 95%) with the remainder being non-collagenous proteins. The remaining 70% of bone is made up of the inorganic mineral hydroxyapatite. This inorganic component ($[\text{Ca}_3(\text{P})_4]_3 \cdot \text{Ca}(\text{OH})_2$) is predominantly crystalline, though may be present in amorphous forms. The mechanical properties of different bones are compared to some commonly used bone replacement materials in Table 1. The scaffold should serve as a temporary material with similar mechanical properties to that of the bone it is replacing. A stress-strain curve of trabecular bone is shown in Figure 1.

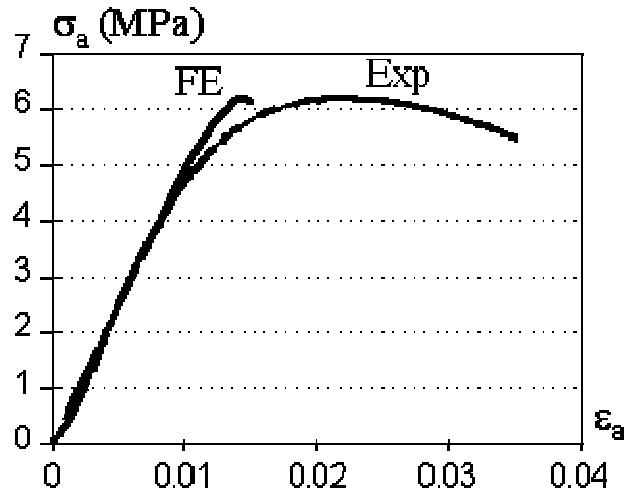


Figure 1: Stress-strain curve of trabecular bone

Table 1: Mechanical Properties of Bone Compared to Bone Replacement Structures

	Direction of Test	Modulus of Elasticity (GPa)	Tensile Strength (MPa)	Compressive Strength (MPa)	% Strain at Break	Reference
Leg Bones	Longitudinal					Sujata, 2002
Femur		17.2	121	167	-	
Tibia		18.1	140	159	-	
Fibula		18.6	146	123	-	
Arm Bones	Longitudinal	17.2-18.6	130-149	114-132	-	Sujata, 2002
Vertebrae	Longitudinal	0.09-0.23	1.2-3.7	1.9-10	-	Sujata, 2002

*Bhat, Sujata. (2002) Biomaterials. Kluwer Academic Publishers

Another crucial requirement of the scaffold is that the internal structure should accommodate vascularization and cells from the local environment (osteoconductivity) and guide deposition of bone in a way that ultimately mimics normal bone. Normal bone possesses an inherent capacity for self repair and regeneration due to the local environment of osteoprogenitor cells, osteoinductive proteins, and blood vessels (Yaszemski *et al.*, 1996). When bone is fractured, the repair and remodeling phases initiate an intricate cellular communication network of osteoblasts and osteoclasts. Osteoblasts synthesize an intermediate collagenous framework and then ossification of this matrix occurs to form new woven bone. The bone undergoes

sequential resorption and deposition that ultimately form the mineral and organic phases of bone (Yaszemski *et al.*, 1995). The formation of an organized mineralized matrix is in the direction of the previous intermediate matrix as a result of the local stresses applied to it (Yaszemski *et al.*, 1995). It should be noted that during ossification, most of the mineral that is deposited forms by growth on existing crystals. There are, however, diseases and injuries that prevent this process of osseous self repair. The scaffold then acts as a template to guide tissue ingrowth.

As a result, the macrostructure of the material is an important characteristic because it determines the extent of vascularization and cell growth. Interconnectivity, porosity, and pore size are thus correlated with bone ingrowth. In general, the minimum requirement of pore size is 100 μm in diameter depending upon implant location and cell sizes (Kim *et al.*, 2004). Studies by Jones *et al* found that at pore sizes of 75 μm , the deposition of mineral salts was hindered. More mineralized tissue was observed at pore sizes $>300 \mu\text{m}$ (Kim *et al.*, 2004). An interconnected porous network promotes permeability of nutrients and gases to the cells and removes wastes by introducing a vascular supply into the scaffold.

The structure should be similar in size and shape to the native tissue/organ and also be highly porous. This brings cellular precursors to the reconstructed area and promotes their adhesion, migration, proliferation, and differentiation. The morphology and architecture of the scaffold should be reproducible and homogenous.

The drive to create biomaterial alternatives that conform to some of the above criteria has lead to the development of several scaffolds used in bone repair. Scaffolds that have been explored for orthopedic applications include synthetic and natural polymers, ceramics, and composites. Table 2 provides examples of common materials in each of these classes of materials that are being explored as bone graft substitutes.

Table 2: Bone Replacement Materials

Classes of Materials	Examples	Reference
Synthetic Polymers	Polyesters: poly(lactic acid (PLA), poly(glycolic acid) (PGA), their copolymer poly(lactic-co-glycolic acid) (PLGA); poly(ethylene glycol) (PEG); polyanhydrides	Yaszemski (1995), Saito (2002)
Natural Polymers	Collagen, hyaluronic acid derivatives, chitosan	Xu (2004)
Ceramics	Hydroxyapatite (HA) $\text{Ca}_{10}(\text{PO}_4)_6\text{OH}_2$, tricalcium phosphate (TCP), biphasic calcium phosphate (BCP), bioactive glasses, calcium sulfate	Yaszemski (1995), Bucholz (1987), Laurencin (1999)
Composites	HA/PLA, HA/chitosan	KiKuchi (1997), Hockin (2005)

3. Synthetic Bone Graft Substitutes

Calcium phosphates (CaPs) have been used as a scaffold to guide and regenerate bone tissue. CaPs are of interest as a substitute because of their similarity to the mineral component of bone (Bohner, 2000). Research has also shown that CaP materials used as bone substitutes are biocompatible, bioactive, biodegradable and osteoconductive (Jarcho, 1981 & Rey, 1990). The strong biocompatibility is directly related to its similarity in composition to bone. Natural hydroxyapatite (HA) is found in 45% of the total bone mass (Laurencin *et al.*, 1999). Calcium phosphate ceramics also offer a potentially limitless availability and eliminate the need for a second morbidity site. Additionally, the macrostructure is similar to trabecular bone and provides a substantial interconnected pore system that promotes vascularization and tissue ingrowth (Laurencin *et al.*, 1999).

Currently, the major calcium phosphate ceramics include β -tricalcium phosphate (β -TCP) which is widely used in the forms of powders, granules, or blocks, and hydroxyapatite (HA), $\text{Ca}_{10}(\text{PO}_4)_6\text{OH}_2$, which is highly crystalline, osteoconductive and is the most stable CaP at neutral pH (Gauthier *et al.*, 1999 & Bohner, 2000). β -TCP ($3 \text{Ca}_3(\text{PO}_4)_2$) has been shown to

degrade faster than HA. More recently, biphasic calcium phosphate (BCP) has been employed to overcome HAs limited bioactivity by combining it with β -TCP in adequate ratios, usually 60% HA and 40% β -TCP (Bohner, 2000).

Despite its osseointegration capabilities and its chemical and crystallographic similarity to the carbonated apatite in normal bone, CaPs brittleness and poor mechanical properties limit their use to non-stress applications (Xu *et al.*, 2004). The newly implanted ceramic lacks immediate structural support due to its low compressive and tensile strength. As a result, researchers have investigated the application of composites, CaPs mixed with polymers such as hydroxy-propyl-methyl-cellulose and poly-L-lactic acid, and also as coatings on metallic implants (Gauthier *et al.*, 1999 & Kikuchi *et al.*, 1997).

Polymers provide flexibility in their design due to their composition and structure. This makes them an attractive material because their physical and chemical properties can be tailored to elicit a specific function. In addition, unlike the slow degrading ceramics that persist for months after implantation, polymers are biodegradable. Polymers that have been investigated in orthopedic applications for bone augmentation in load bearing applications are shown in Table 3. The effectiveness of a polymer as a scaffold in regards to bone regeneration is briefly described in comparison to other polymers.

Table 3: Properties of Selected Synthetic Biodegradable Polymers

Polymer	Advantages	Disadvantages	Authors
Polyesters	Extensively studied, adjust degradation rate, easily processed,	Weak mechanical properties, can have toxic by-products, bulk degradation	Agrawal, 2000 Taylor., 1994
Polyanhydride	Rapid and well defined surface erosion, surface erosion	Poor mechanical properties	Agrawal, 2000
Polyorthoester	Degrades by surface erosion	Weak mechanical properties	Agrawal, 2000
Polycaprolactone	Slower degradation rates in comparison	Insufficient mechanical properties	Agrawal, 2000
Polycarbonate	Less immunogenic	Toughness up to 140°C	Agrawal, 2000
Polyfumarate	Mechanical properties similar to trabecular bone		Agrawal, 2000

Polymeric scaffolds used for bone augmentation present several limitations. It is evident in Table 3 that a common disadvantage of polymers is poor mechanical properties. The most extensively used synthetic polymers in biomedical applications are the polyesters such as poly-L-lactic acid or poly(lactic-co-glycolic acid). However, some polyester polymers present major disadvantages. They degrade fast relative to the amount of time it takes for host tissue to regenerate. This is a result of their hydrophilic nature which causes them to degrade by a bulk degradation mechanism. Such degradation denotes mass loss, which changes the structure of the scaffolds, and ultimately leads to a collapsed template therefore eliminating the structural support necessary to promote normal bone regeneration. Thus the mechanical properties initially prescribed to the polymer early on in the degradation process are reduced. They also tend to be

too elastic and do not exhibit osteoconductive properties. The initial mechanical properties of some of the bioresorbable polymers used are shown in Table 4.

The products of degradation have also raised concern in relation to toxicity. Although polymers have proved to be biocompatible, bulk degradation polymers tend to result in an acid burst that can result in inflammation. Studies to address these concerns were conducted by Taylor *et al.* in 1994. PLA and PGA, along with four other polymers, were studied over 16 weeks. Toxicity, rates of degradation, and toxicity of degradation components were determined. The degradation products of PGA and PLA were toxic at 10 days and 4 weeks respectively.

Table 4: Mechanical Properties of Select Biodegradable Polymers

Polymer (MW)	Tensile Strength (MPa)	Tensile Modulus (MPa)	Flexural Modulus (MPa)	Elongation Yield/Break (%)
PGA (50,000)	-	-	-	-
L-PLA (50,000)	28	1200	1400	3.7/6.0
D,L-PLA (107,000)	29	1900	1950	4.0/6.0
Polyanhydride				
Poly(CPP- SA-ISO) (31,000)	-	-	-	-
Poly (SA-HAD) (142,000)	4	45	-	14/85
Polyorthoester				
DETOSU:t-CDM:1,6-HD (99,700)	20	820	950	4.1/220
Polycaprolactone				
(44,000)	16	400	500	7.0/80
Polycarbonate				
Poly(BPA-imino) (105,000)	50	2150	2400	3.5/4.0
Poly(DTH-imino) (101,000)	40	1630	-	3.5/7.0

* Agrawal *et al.*, 2000

Composites were developed to overcome limitations of using ceramics and polymers independently. Ceramics are brittle and osteoconductive and polymers are flexible, biodegradable, and have no osteoconductivity. By combining the two with the following characteristics, the osseointegration and biocompatibility of the material is improved. In addition, the mechanical properties are improved (Kikuchi *et al.*, 1997)

4. *Natural Bone Graft Substitutes*

Collagen has been utilized as a bone template scaffold because it exhibits important mechanical. It is additionally believed to be promising due to the fact that natural bone is composed of mainly type II collagen. It is biocompatible and can be genetically manipulated for control purposes (Meinel *et al.*, 2004). However, studies show that the fast degradation rate of collagen prevents substantial calcification and causes the structure to collapse. An *in vitro* study by Meinel *et al.* demonstrated that by four weeks of culture, calcium deposition in the collagen scaffold had significantly decreased. This was attributed to the degradation of the scaffold since there was progression between 2-4 weeks (Meinel *et al.*, 2004).

Today, collagen is one of the most widely used biomaterials for scaffolds. However, they have limited options for engineering control of structure and thus limited mechanical function. This is due to the primary sequence containing essentially one repetitive block (Gly-Pro-HyP) that is well conserved (Kaplan, 2000)

Although the synthetic and natural bone substitutes discussed provide many important benefits, they still present disadvantages that keep the medical world in search of new alternatives. A brief overview of the advantages and disadvantages of clinical bone grafts and bone replacement substitutes are shown in Table 5. It is evident that the structural support and

mechanical integrity of scaffolds becomes a problem in bone tissue engineering. The mechanical properties of some of the commonly used bone replacement materials discussed above are presented in Table 6.

Table 5: Comparison of Bone Graft Materials

Graft	Properties	Advantages	Disadvantages
Autograft	Osteogenic, osteoinductive, osteoconductive	No host rejection, no disease transmission, retains viable osteoblasts	Second donor-site morbidity, limited availability, costly
Allograft	Osteoconductive, weakly osteoinductive	Greater availability than autograft, customized forms available, no additional surgical procedure	Immunogenic, disease transfer risk, not osteogenic, expensive
Ceramics (TCP, HA)	Osteoconductive	Limitless availability, no additional surgical procedure, similar composition to bone	Not osteogenic or osteoinductive, weak immediate mechanical support, difficult fabrication process, brittle
Collagen		Favorable matrix to bone regeneration	Minimal structural support, potentially immunogenic
Demineralized Bone Matrix (DBM)	Osteoconductive, osteoinductive	Ease of use, no additional surgical site	No structural support, not osteogenic
Synthetic polymers		Low density, Easy to fabricate	Low mechanical strength, not osteoconductive, may cause tissue reaction

Abbreviations: TCP= tricalcium phosphate, HA= hydroxyapatite *Adopted from Kaplan, 2000

Table 6: Mechanical Properties of common bone replacement structures

	Modulus of Elasticity (GPa)	Tensile Strength (MPa)	Compressive Strength (MPa)	% Strain at Break	Reference
HA	7-13	38-48	350-450	-	Bhat, 2002
PGA	8.4	890	-	30	Bhat, 2002
PLA	1.2-3.0	28-50	-	2-6	Altman, 2002
Collagen	0.0018-0.046	0.9-7.4	-	24-68	Altman, 2002

*Bhat, Sujata. (2002) Biomaterials. Kluwer Academic Publishers

Abbreviations: HA= hydroxyapatite, PGA=polyglycolic acid, PLA=polylactic acid with molecular weights ranging from 50,000-300,000, Collagen= rat tail collagen Type I extruded fibers tested after stretching from 0-50%

A reoccurring weakness presented in Table 5 with many of the synthetic and natural structures used for bone regeneration is the absence of osteogenic or osteoinductive properties. The mechanical integrity of the scaffolds also becomes a problem when introduced into the unique osseous environment (stress/strain/compression).

It can be concluded that in order to effectively tissue engineer bone, the following minimum requirements should be met: 1) an appropriate 3-D, porous substrate must be used to ensure cell attachment, growth, and differentiation, and ECM production and to promote nutrient and waste exchange; 2) provide optimal mechanical properties that match and support those of native tissues; 3) biodegradable, biocompatible and resorbable characteristics; 4) allow for bioactive molecule delivery, and have a suitable surface chemistry; 5) a reproducible architecture to maintain homogeneity. The common matrices used in bone tissue engineering have been evaluated, and their shortcomings have proved that there is not an ideal bone scaffold as of yet. Most scaffolds reported only conform to a few of the criteria discussed. Therefore, there is a need for new biomaterials that are capable of inducing bone formation. To meet the challenging

native environment of bone as well as meet the challenging scaffold requirements, researchers have been exploring silks with their unique mechanical and functional properties.

6. *Silk Scaffold for Bone Formation*

Silks are generally defined as spun fibrous protein polymer secretions synthesized by a variety of organisms including silkworms, spiders, scorpions, mites and flies. Silk fibers are usually spun into the air; however, some aquatic insects produce silks spun under water (Zhao *et al.*, 2002). Silks differ in composition, structure, and properties depending on the specific source. The mechanical properties are tailored to the specific functions of the silk. They are known to have a wide range of native functions such as high strength netting to entrap insects and the protective membranes that prevent environmental harm. Other functions include reproduction as cocoon capsular structures, web construction and adhesion, and lifeline support (Altman *et al.*, 2002). The most extensively characterized silks are from silkworm, *Bombyx mori*, and from spiders, *Nephila clavipes* and *Araneus diadematus* (Altman *et al.*, 2002).

Fibrous proteins are characterized by a highly repetitive primary sequence which leads to significant homogeneity in secondary structure. The organization of the primary structural components from a range of lepidopteran silk and one arachnid are shown in Figure 2. The primary structural sequence consists of a central repeating unit containing mostly hydrophobic amino acids that are interspersed with a more complex hydrophilic, amorphous region. This region is referred to as a “spacer” and is less than one tenth the size of the hydrophobic regions (Altman *et al.*, 2002 & Bini *et al.*, 2004). The N- and C-termini regions are non-repetitive and hydrophilic in nature. The sizes of these termini in a variety of silks are shown in Table 7. Additionally, this table summarizes other components of fibroin primary sequences. It should be

noted that although there is variability among silks, the organization of the components is similar.

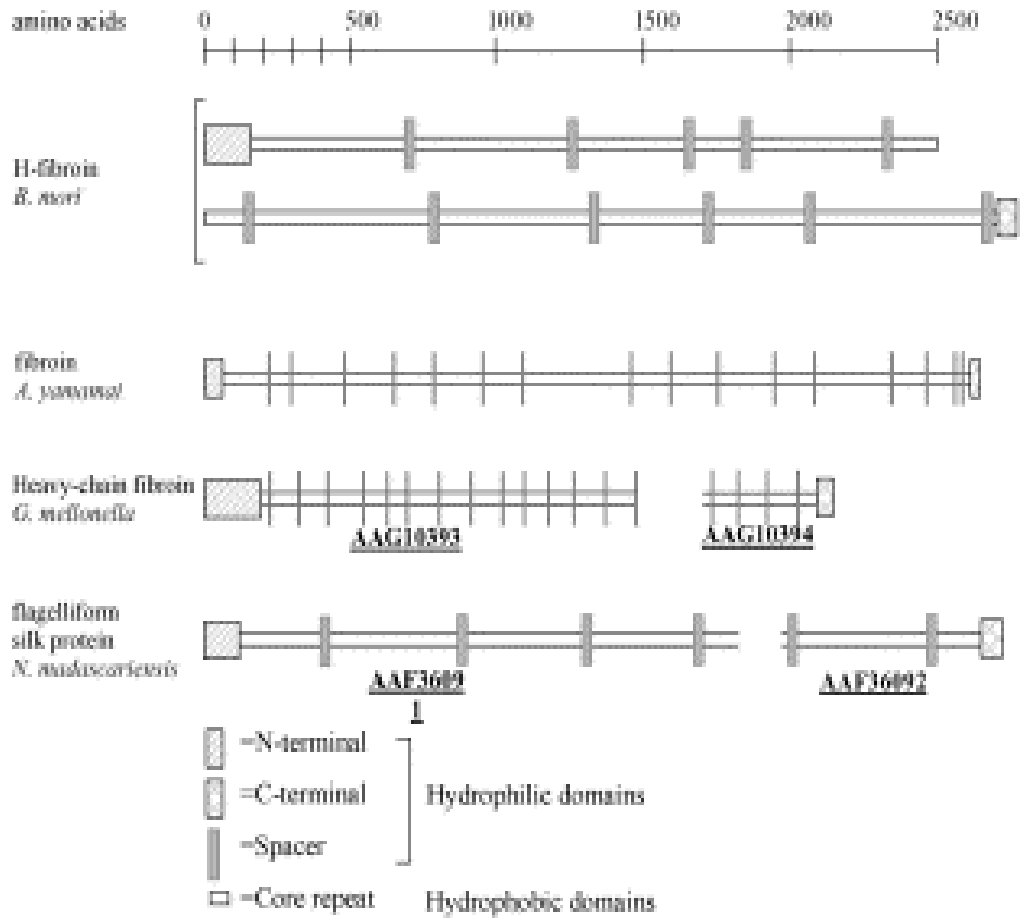


Figure 2: Organization of hydrophilic and hydrophobic domains in silk proteins. Shown is the heavy fibroin chain of *B. mori*, *A. yamamai*, heavy fibroin chain of *G. mellonella*, and *N. madagascariensis* as indicated by respective fragments. *(Bini *et al.*, 2004)

Table 7: Summary of Components of Hydrophilic and Hydrophobic Components of fibroin Sequences

Sequence	Hydrophilic blocks					Hydrophobic blocks			
	N-term size (aa)	C-term size (aa)	Size of hydrophilic spacer (no.aa) & representative sequence	Ratio N-term aa: spacer aa	Ratio C-term spacer aa	Range (no. aa)	Average (no. aa)	No. of blocks	Core Repeat Sequence
Lepidoptera									
<i>Bombyx mori</i>	151	50	32-33, TGSSGRGPY VGGYSG	4.7	1.5	159-607	425.7	12	*Shown below
<i>Bombyx mandarina</i>	151	^b	YEYAWSSE						
<i>Antheraea mylitta</i>	86	^b	SDFGTGS						
<i>Antheraea pernyi</i>	87	32							
<i>Antheraea yamamai</i>	87	32	7, RRAGYDR	12.4	4.5	140-340	149.6	16	
<i>Galleria mellonella</i>	189	60 ^c	6-8 EVIVIDDR	27	9.5	75-99	89.38	13 ^d	
Arachnida									
Flagelliform									
<i>Nephila clavipes</i>	115	89 ^c							
<i>Nephila madascariensis</i>	115	89 ^c	26, TTIIEDLDITI DGADGPI	3.4	4.4	260-380	341.5	5 ^d	
Major ampullata									
<i>Nephila clavipes</i>	^a	97	No spacer			19-46			
<i>Gasteracantha mammosa</i>	^a	89	No spacer						
<i>Argiope aurantia</i>	^a	82	No spacer						
<i>Nephila senegalensis</i>	^a	82	No spacer						
<i>Latrodectus geometricus</i>	^a	88	No spacer						
<i>Araneus diadematus</i>	^a	94	No spacer						

^a N-terminal sequences of these proteins were not available.

^b C-terminal ends not available.

^c N- and C-terminal were obtained from two fragments of the sequence. These were *G. mellonella*, *N. clavipes*, and *N. madascariensis*

^d Sequences were incomplete. Number of blocks, average size and ranges were based on the fragments available

Table 7 cont: *Core Repeat Sequence

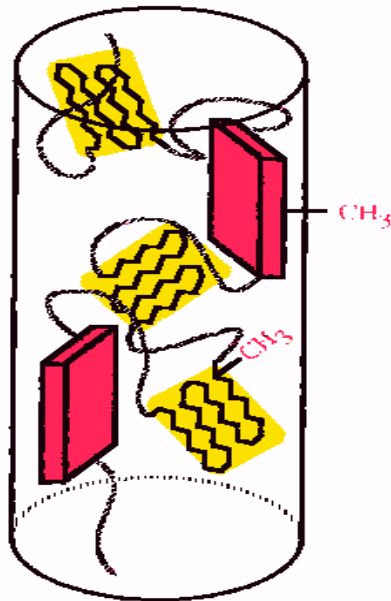
	<i>Bombyx mori</i>	<i>Antheraea yamamai</i>	<i>Galleria mellonella</i>	<i>Nephila madascariensis</i>	<i>Nephila clavipes</i>
Core Repeat Sequence	(GAGAGS) ₅₋₁₅ , (GX) ₅₋₁₅ , (X=V, I, A,), GAAS	(S ₁₋₄ A ₁₁₋₁₃), GX ₁₋₄ GGX, GGGX (X=A, S, Y, R, DV, W, R, D	(S ₁₋₂ A ₁₋₄) ₁₋₂ GLGGLG, GXGGXG (X=L, I, V, P), GPC (X=L, Y, I)	(GP(GGX)1-4Y) _n (X=Y, V, S, A), GRGGAn, GGX _n (X=A, T, V, S)	GAG(A) ₆₋₇ GGA, GGX GXGXX (X=Q, Y, L, A, S, R)

*Adopted from Bini *et al.* 2004

The secondary structure of the fibrous protein can consist of either helical, β -sheet (chain axis is parallel to the fiber axis) or cross- β -sheet (chain axis is perpendicular to the fiber axis) (Valluzi *et al.*, 2002). Both the spider dragline silk from *Nephila clavipes*, and the silkworm silk *B. mori*, are characterized by a secondary structure of β -pleated-sheets, as is the case for most silks (Valluzi *et al.*, 2002). Polypeptide chains are extended from the β -pleated-sheet structure in which the carbonyl oxygens and amide hydrogens are at near right angles to the long axis of the chain. The carbonyl oxygens form hydrogen bonds with the amide hydrogens on neighboring chains resulting in a pleated structure along the backbone of the peptide chain. There is extensive hydrogen bonding in silk as well as van der Waals interactions for stacked sheets due to the dominant amino acids such as glycine, alanine, and serine (Valluzi *et al.*, 2002).

Generally, spider dragline and silkworm silks are considered semicrystalline materials with amorphous flexible chains reinforced by strong crystals. The crystalline regions (β –sheets) throughout the silk are very hydrophobic and consist of highly ordered protein crystals of alanine or alanine-glycine peptides (Kaplan, 1998). This gives silk a combination of stiffness and strength. Silk's elastic property is a result of the disordered, loose, coil-like protein chains of glycine peptides which aggregate to form the amorphous regions. Less ordered alanine-rich

crystalline regions have also been identified and believed to connect the amorphous regions with the β -sheets. The structural properties of the various silks depend on the composition and arrangement of these proteins. The crystalline and amorphous regions are shown in Figure 3.



*Zhao *et al.* (2002)

Figure 3: Schematic organization of crystalline and amorphous regions in a silk fiber. The red and yellow blocks represent the crystalline and amorphous regions respectively. The black canted sheet-like structures are weakly oriented, yet crystalline. Not drawn to scale, in reality the glycine-rich amorphous regions compose about 70% of the fiber.

In silkworm fiber, the β -sheets consist of the glycine-alanine crystalline repeats. All of the crystalline regions in spider dragline fibers, in addition to the silkworm *Antheraea pernyi*, are composed of alanine-rich sequences. The amino acid compositions of four different silk species are shown in Table 8. Generally, the crystalline regions are interspersed by domains of 34-40 amino acids that make up the non-crystalline, or amorphous, regions of the protein. The proportions of crystalline and amorphous regions in the silk depend on the type of silk. Protein

crystals account for 40-50% of *B. mori* silk and 15% of silks produced by the major ampullate when hydrated (Craig *et al.*, 2002).

Table 8: Amino acid composition of silk fibroin and one glue protein (mol%) from four different species

Amino acids	<i>B. mori</i> fibroin	<i>B. mori</i> sericin	<i>S.c. ricini</i> fibroin	<i>A. pernyi</i> fibroin	<i>A. yamamai</i> fibroin
Gly	42.9	13.5	33.2	26.7	26.1
Ala	30	5.8	48.4	48.1	48.1
Ser	12.2	34	5.5	9.1	9
Tyr	4.8	3.6	4.5	4.1	3.9
Asp	1.9	14.6	2.7	4.2	4.5
Arg	0.5	3.1	1.7	2.9	3.5
His	0.2	1.4	1	0.8	0.8
Glu	1.4	6.2	0.7	0.8	0.7
Lys	0.4	3.5	0.2	0.2	0.1
Val	2.5	2.9	0.4	0.7	0.7
Leu	0.6	0.7	0.3	0.3	0.3
Ile	0.6	0.7	0.4	0.4	0.4
Phe	0.7	0.4	0.2	0.3	0.2
Pro	0.5	0.6	0.4	0.3	0.4
Thr	0.9	8.8	0.5	0.5	0.6
Met	0.1	0.1	Trace	Trace	Trace
Cys	Trace	0.1	Trace	Trace	Trace
Trp	-	-	0.3	0.6	0.7

*Adopted from Zhao *et al.*, 2001

Silks are produced in modified salivary glands for both the Lepidoptera and Diptera.

Spiders, however, produce silks in multiple glands and typically use more than one type of silk to make their nests, traps and cocoons (Craig *et al.*, 2002). A list of selected species (there are over 34,000 species of spiders) and the corresponding gland that produces the silk is listed in Table 9.

Table 9: List of Lepidoptera, Diptera, and spider species and their silk producing gland

Species	Producing Gland
Lepidoptera & Diptera	
<i>Antheraea pernyi</i>	Salivary
<i>Antheraea yamamai</i>	Salivary
<i>Galleria mellonella</i>	Salivary
<i>Bombyx mori</i>	Salivary
<i>Bombyx mandarina</i>	Salivary
<i>Antheraea mylitta</i>	Salivary
<i>Chironomus tentans</i>	Salivary
Spiders	
<i>Nephila clavipes</i>	Major ampullate
<i>Nephila senegalensis</i>	Major ampullate
<i>Gasteracantha mammosa</i>	Major ampullate
<i>Argiope aurantia</i>	Major ampullate
<i>Araneus diadematus</i>	Major ampullate
<i>Latrodectus geometricus</i>	Major ampullate
<i>Araneus bicentenarius</i>	Major ampullate
<i>Tetragnatha versicolor</i>	Major ampullate
<i>Araneus ventricosus</i>	Major ampullate
<i>Nephila Clavipes</i>	Minor ampullate
<i>Dolomedes tenebrosus</i>	Ampullate
<i>Euagrus chisoseus</i>	Combined
<i>Plectreurys tristis</i>	Larger ampule-shaped
<i>Argiope trifasciata</i>	Flagelliform
<i>Nephila madagascariensis</i>	Flagelliform
<i>Nephila clavipes</i>	Flagelliform

* Adopted from Bini *et al.*, 2004

All of the organisms that produce silk synthesize task specific silk with divergent mechanical properties depending on its function (Scheibel, 2004). Adult spiders have seven different types of glands that yield four fibroin silks and three types of protein glue (Craig *et al.*, 2002). The type, function, and mechanical properties of spider silk and silkworm silk are shown in Table 10. For the purpose of the paper, only the glands that produce the fibroin silks are discussed.

Table 10: Comparison of extensibility, elastic modulus, and tensile strength of silks

Silk	Silk Gland	Function	Extension (%)	Elastic modulus (GPa)	Tensile strength (kpsi)	References
Dragline	Major ampullate	Orb web frame, radii, ampullate	35	10-50	400	Kaplan, 1997
Minor	Minor ampullate	Orb web frame	5	*	100	Kaplan, 1997
Viscid	Flagelliform	Prey capture, sticky spiral	200	*	100	Kaplan, 1997
Cocoon	Cylindrical (tubuliform) Salivary	Reproduction	*	*	*	Kaplan, 1997

Major and minor ampullate silk values are for *N. clavipes*. Similar values were found with silk from *Areneus gemmoides*. Flagelliform silk values are for *Araneus diadematus*. *Indicate that the values were not found.

Most silks assume different secondary structures at different points during the *in vivo* processing. In general, there are two distinct structures categorized as Silk I and Silk II. Before spinning, the silk proteins are water-soluble with high molecular weights (Silk I). They are stored at high concentrations in their respective glands. This protein solution forms the silk dope which displays properties of a liquid crystal. In this state, the peptide motifs are thought to adopt an α -helical conformation, β -turns, or random coil conformation. In spider dragline, the polyalanine motifs adopt an α -helical conformation, while the glycine-rich motifs form either β -turns or random coil conformation (Scheibel, 2004).

The protein liquid crystal solution passes through the narrowing tubes of the spinning duct in both spider and silkworm glands. Here, water, sodium, and chloride are extracted from the solution. The pH is also lowered and initiates partial unfolding of the proteins. The silk proteins slightly extend, align, and pack much closer together (Scheibel, 2004). Partial

crystallization occurs parallel to the fibre axis. In spider dragline, as the hydrophobic polyalanine segments of the silk align, they are exposed to an increasingly hydrophobic environment, triggering their conversion from α -helical to β -pleated sheet structures (Scheibel, 2004). After spinning, it is then converted into water-insoluble fibers (Silk II) (Kaplan, 1997).

Silk proteins exhibit impressive mechanical properties that have been shown to exceed that of high performance fibers such as Kevlar (Altman *et al.*, 2002). Table 11 shows the mechanical properties of *B. mori* silk and spider dragline silk from *N. clavipes* (which is regarded as nature's high performance fiber) and compares them to other materials.. The stress-strain curve for *B. mori* silk is shown in Figure 4. The highly organized structure of silk contributes to its mechanical properties

Research has shown that the amphiphilic nature of the protein is responsible for the mechanical properties of silks having a unique combination of both strength and toughness (Altman *et al.*, 2002). The predominantly hydrophobic nature of the crystalline regions is essential to exclude water and in turn produce a high packing density of β -sheet crystals that are believed responsible for the high strength and stiffness associated with the fiber, while the elasticity of the silk fibroin arises from the amorphous domain (Zhao *et al.*, 2002). This also explains why the silk is water insoluble, in which the water molecules are unable to penetrate the strongly bonded β -sheets. In addition, unlike globular proteins, silk fibers have extensive hydrogen bonding. These properties provide silk fibers with superior environmental stability (Altman *et al.*, 2002).

Table 11: Mechanical properties of silkworm and dragline silk compared to other materials

Material	UTS (MPa)	Modulus (GPa)	% Strain at break	Authors
<i>B. mori</i> silk ^a (w/ sericin)	500	5-12	19	Perez-Rigueiro <i>et al.</i>
<i>B. mori</i> silk ^b (w/o sericin)	610-690	15-17	4-16	Perez-Rigueiro <i>et al.</i>
<i>B. mori</i> silk ^c	740	10	20	Cunniff <i>et al.</i>
Spider silk ^e	875-972	11-13	17-18	Cunniff <i>et al.</i>
Collagen ^f	0.9-7.4	0.0018-0.046	24-68	Pins <i>et al.</i>
Collagen X-linked ^g	47-72	0.4-0.8	12-16	Pins <i>et al.</i>
PLA	28-50	1.2-3.0	2-6	Engelberg and Kohn
Tendon (comprised mainly of collagen)	150	1.5	12	Gosline <i>et al.</i>
Kevlar (49 fiber)	3600	130	2.7	Gosline <i>et al.</i>
Synthetic Rubber	50	0.001	850	Gosline <i>et al.</i>

*Altman *et al.*, 2003

^a *Bombyx mori* silkworm silk: determined from bave (multithread fibers naturally produced from silk worm coated in sericin).

^b *Bombyx mori* silkworm silk: determined from single brins (individual fibroin filaments following extraction of sericin).

^c *Bombyx mori* silkworm silk: average calculated from data in Cuniff, 1994.

^d *Nephila clavipes* silk produced naturally and through controlled silking.

^e Rat-tail collagen Type I extruded fibers tested after stretching from 0% to 50%.

^f Rat-tail collagen dehydrothermally cross-linked and tested after stretching from 0% to 50%.

^g Polylactic acid with molecular weights ranging from 50,000 to 300,000.

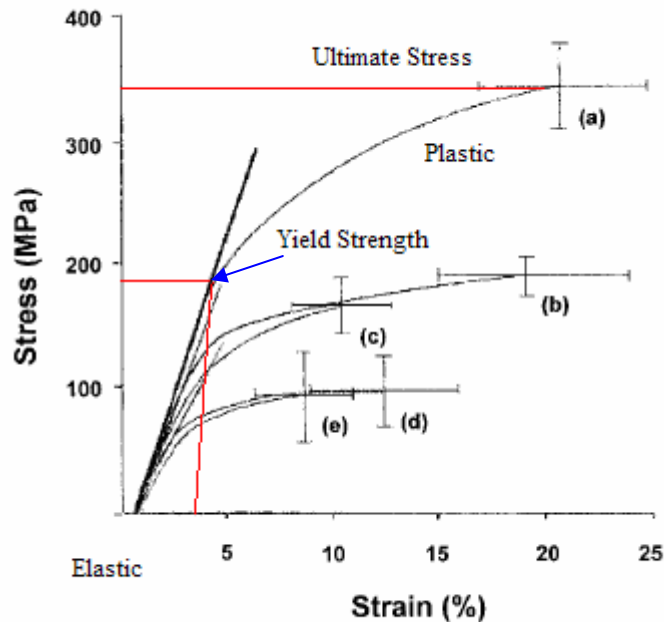


Figure 4: Stress-strain curves of (a) native *B. mori* silk fibroin fiber and (b)-(e) regenerated *B. mori* fibroin fibers after postspinning treatments. The cross signs represent the experimental errors. *Adopted from Zhao *et al.*, 2002

In the stress-strain curve, the silk material will not relax to its initial shape after the force is removed once it is past the elastic limit. Looking at only curve (a), the elastic limit is underneath the area before the line begins to curve. This is the point where the deformation (strain) of the material is irreversible (Zhao *et al.*, 2002). This occurs in between the elastic and plastic regions of the stress-strain curve. The silk material will actually break at the ultimate tensile strength (UTS) (located in the stress-strain curve Figure 4) (Zhao *et al.*, 2002).

B. mori silk has been used commercially as biomedical sutures for decades. Although spider silks have also been well characterized, they have not been used for biomedical applications largely due to the predatory nature of spiders and the low level of production when compared to that of silkworm (Altman *et al.*, 2003). In addition, current research with precise silkworm silk fibers and films suggests that core silk fibroin fibers demonstrate analogous

biocompatibility *in vitro* and *in vivo* with other biomaterials such as collagen (Altman *et al.*, 2002).

In silkworm silk derived from the cocoon of *B. mori*, the fibroin fibers are the core filaments and contain at least two major fibroin proteins. They are the heavy chain fibroin (325 kDA) and a light chain fibroin (25 kDA). *B. mori* also produces a sericin coat that encases the core fibers. It is a glue-like protein that holds the two fibroin fibers together to form the composite fibers of the cocoon case. The sequence of the core repeats in the fibroin heavy chain of the *B. mori* contains alanine-glycine repeats as well as serine or tyrosine (Altman *et al.*, 2002).

A study conducted by Wen *et al.* in 1990, indicated that there were some adverse effects including bioincompatibility and hypersensitivity to virgin silk (fibroin containing sericin gum). The adverse effects were attributed to sericin (Wen *et al.*, 1990). Recent studies demonstrate improved methods that completely extract sericin by boiling the cocoons, removing its antigenic effects. The resulting silk fibroin material produced immunological reactions similar to common biomedical materials such as polyesterene (Meinel, 2003 & Sofia, 2000).

Silk is also an attractive material because of its slow degradation rate. This allows for a temporary scaffold that maintains mechanical integrity until host tissue regenerates. Studies have determined that silk is degradable over a long period of time because of proteolytic degradation often mediated by a foreign body response (Lam *et al.*, 1995, Uff *et al.*, 1995). Most silk fibers lose the bulk of their strength within 1 year *in vivo* and are unrecognizable within 2 years (Altman *et al.*, 2002). Studies performed on silk *in vitro* have shown that proteases cleave the less-crystalline regions of the protein to peptides which are then able to be phagocytosed for additional metabolism by the cell (Asakura *et al.*, 1997). Studies have also demonstrated that

protease cocktails and chymotrypsin are able to enzymatically degrade silk (Asakura *et al.*, 1997).

The highly organized structure of silk not only contributes to its mechanical properties but also affects its degradation. Degradation rate can be altered by changing the content of the β -sheets. A high content of β -sheets causes the silk scaffold to degrade more slowly while a low content degrades fast. This is because more hydrogen bonding provides for closely packed sheets that make it more difficult for water molecules to penetrate and break the bonds. Therefore, by modifying the organizational structure of the β -sheet the degradation rate can be more closely matched with bone tissue ingrowth at the implant site.

Silk fibroin presents versatility in matrix scaffold design for an array of tissue engineering needs (Altman *et al.*, 2002). Scientists are able to process silk fibroin into foams, films, fibers and meshes (Minoura *et al.*, 1995, Altman *et al.*, 2002). The change in morphology and architecture, such as pore size, porosity, and interconnectivity can be controlled based on the mode of preparation (Kim *et al.*, 2004). This is critical to the *in vivo* mechanical behavior of the scaffold. To date, fabrication methods that have been utilized are solvent casting, particulate leaching, freeze-drying, gas foaming, melt molding, and phase separation (Nazarov *et al.*, 2003). The diverse amino acid side chains allow for selective chemical couplings for tissue engineering. Also, it has been demonstrated that silk matrices promote cell attachment, proliferation, and differentiation.

Studies conducted on silk scaffolds demonstrated the dependence of scaffold integrity on such properties as pore size and homogeneity. It was reported that a more uniform pore distribution improved the mechanical properties of the scaffold (Kim, 2004). Stress that is applied to the scaffold is concentrated at the pore interfaces, and if it is not uniform, quicker

deformation will occur as well as a decrease in compressive strength and modulus (Kim *et al.*, 2004).

An example of silk's matrix versatility is evident in research conducted by Dunn *et al.* in 1992. This study demonstrated that silk fibers are superior to collagen fibers and other enhanced scaffolds such as collagen fiber-PLA constructs (Dunn *et al.* 1992). During the study, Dunn *et al.* analyzed the development of a collagenous anterior cruciate ligament (ACL) prosthesis. The results showed inconsistent neoligament formation and considerable weakening of the collagen prosthesis in a rabbit model (Dunn *et al.* 1992). They also utilized enhanced scaffolds such as a collagen fiber-PLA composite in order to maintain mechanical integrity to allow for neoligament tissue ingrowth (Dunn *et al.* 1992). But in both studies, merely half of the structures stayed intact 4 weeks post-reconstruction. This implied that the collagen and PLA composite was insufficient for the demanding *in vivo* environment of the ACL (Dunn *et al.* 1992). However, silk fibroin fibers woven into a wire-rope geometry presented unique mechanical properties similar to that of the native ACL and supported host tissue ingrowth that surpassed that of collagen and the collagen/PLA construct (Altman *et al.* 2003).

As discussed, an attractive characteristic of silk is its diverse amino acid side chains that can be modified. Recent evidence suggests that a silk scaffold decorated with RGD, when compared with other integrin recognition sequences, increased osteoblast differentiation and mineralization *in vitro* (Sofia, 2000).

Other research demonstrates that the incorporation of a RGD peptide in a silk scaffold significantly increased the amount of calcium present after four weeks in culture compared to an undecorated silk scaffold (Meinel, 2004). The void area was completely filled with ECM which consisted of organized parallel collagen bundles and osteoblast-like cells, and few with

fibroblast-like morphology. Both of the silk groups had more calcium deposition than the collagen scaffolds (Meinel, 2004).

This mechanical attachment of the intracellular cytoskeleton of cells to their extracellular matrix is important in modulating a number of cellular functions such as cell proliferation and migration. Integrins accomplish this by recognizing the arginine-glycine-aspartate (RGD) sequence motif located in proteins found in the ECM. RGD is a synthetic peptide that acts as active modulators of cell adhesion. This process is of interest to tissue engineers because it provides a means to control cellular function on a variety of matrices by covalently attaching RGD peptides to the surface of the material.

Incorporating stem cells onto a scaffold has shown promise in generating engineered tissues and organs. Human MSCs have been researched in bone tissue engineering due to their capacity to differentiate into bone-making cells. The type of lineage adopted is dependent on the extrinsic signals from cytokines and other local signals. Direct control of differentiation of hMSCs are currently represented by demonstration of osteoblastic differentiation in various biologically or synthetic derived matrices. These precursor cells are easily isolated and capable of *in vitro* proliferation and differentiation. They can then be cultured on a matrix *in vitro* prior to implantation to repair the defect or implanted immediately upon seeding (Pittenger *et al.*, 1999).

Human MSCs seeded on silk films and silk films covalently bound to the amino acid sequence (RGD) both *in vitro* and *in vivo* was studied by Meinel *et al.* The *in vitro* analysis compared cells grown on tissue culture plastic (TCP; negative control), TCP coated with lipopolysaccharide (LPS; positive control) and collagen films. The hMSCs formed monolayers on both of the silk films and clustered on the collagen film. Cell proliferation was significantly higher on the silk films compared to the collagen or TCP. These findings were substantiated by

in vivo studies in which the silk films, collagen film, and a PLA film were implanted intramuscularly into the quadriceps, triceps and rectus abdominus muscles (Meinel *et al.*, 2004). Cell proliferation was advanced on the silk films, particularly on silk with RGD (Meinel *et al.*, 2004).

A study conducted by Meinel *et al* in 2004 substantiated the suitability to attach hMSCs to silk in order to promote bone formation. Both silk and collagen scaffolds were studied with the same microstructure. When cultured on the silk, stem cells expressed strong transcript levels of all three bone markers studied: bone sialoprotein (BSP), osteopontin and BMP-2. They also accumulated bone-like matrix containing alkaline phosphatase and mineral. The bone formation resulted in interconnected trabeculae of bone-like tissue. Collagen scaffolds could not generate similar outcomes as a result of its rapid degradation.

Research has also demonstrated that the osteogenic potential of a scaffold can be improved by incorporating certain bioactive molecules known to induce bone formation. Osteogenic molecules, particularly of the transforming growth factor (TGF)- β superfamily, play a key role in bone formation and repair.

Other osteoinductive bioactive molecules that are involved in new bone formation and remodeling include: 1) insulin-like growth factors (IGF); 2) skeletal growth factors (SGF); 3) transforming growth factors (TGF); 4) osteoblast derived growth factors (BDGFs); 5) epidermal growth factors; 6) vascular endothelial growth factors; 7) bone morphogenetic proteins (BMPs). Although BMP is one among a list of growth factors, it is the only one that is capable of transforming connective tissue cells into osteoprogenitor cells.

BMPs induce undifferentiated mesenchymal cells to differentiate through the chondrogenetic or osteogenetic pathway. This can result in bone formation in non-osseous

environments. The BMPs accomplish this by forming a complex of two different types of serine/threonine kinase receptors: type I and type II. The receptors are induced at physiological and pathological ossification sites and are essential in the development of new bone. Once ligands bind to both the receptors, phosphorylation of type I occurs by type II. This phosphorylation results in an increase of specific molecules in the cell cytoplasm such as alkaline phosphatase and collagen synthesis.

Bone morphogenetic proteins (BMP), including BMP-2-15, are members of the TGF- β superfamily and were initially identified as bioactive molecules in the demineralized bone matrix, discovered by Marshall Urist in 1965 (Sykaras *et al.*, 2001). These can be further divided into three different subfamilies: BMP-2, BMP-3, and BMP-7. There have been over 15 BMPs cloned and expressed in humans and mice. The TGF- β superfamily is an assemblage of multifunctional cytokines which have vital roles in development and in the regulation of differentiation and proliferation of mesenchymal stem cells, including cartilage and bone formation (Scheufler *et al.*, 1999). The cytokines act on mesenchymal cells in a concentration-dependent manner, and are based on thresholds.

The different isoforms of BMP have different roles in developmental processes during embryogenesis and during repair. For example, BMP 2-7 induce bone formation and differentiation. Bone morphogenetic protein-2 (BMP-2) is one of the key representatives of the collection of bone morphogenetic proteins (Scheufler *et al.*, 1999). BMP-2 is synthesized as a 453 amino acid proprotein which is glycosylated, proteolytically cleaved and dimerized to result in a mature homodimeric protein consisting of 114 C-terminal proprotein residues (Scheufler *et al.*, 1999). The dimensions of the dimer are 70 Å x 35 Å x 30 Å.

Each monomer contains a cystine-knot that is assembled from six cystine residues, with three intrachain disulfide bridges. Comparable cyseine-knots have been discovered in transforming growth factors, vascular endothelial growth factor, platelet derived growth factor, β nerve growth factor, brain-derived neurotrophic factor as well as gonadotropin (Scheufler *et al.*, 1999). Because the proteins of this BMP family lack the familiar hydrophobic core that globular proteins contain, the cystine-knot scaffold is important in order to stabilize the structure. BMP-2 stabilizes itself additionally by dimerization, where a hydrophobic core is generated between the monomers (Scheufler *et al.*, 1999).

Protein-based polymers, specifically silks, are logical choices for scaffolding for the formation of bone. It can be concluded from the literature that the reasons for the optimism are many-fold. Some of the reasons discussed included: 1) the natural role of the structural proteins of silks in tissue remodeling, including collagens in the ECM; 2) its biocompatibility (silks have been used as sutures) with potential resorbable properties; 3) the mechanical integrity (unique stress/strain/compression); 4) silks can be processed through varying techniques with the ability to control architecture; 5) suitable surface chemistry that can be decorated with a direct level of control (as shown through extensive research); 6) the ability to self-assemble. These important controls of polymer structure can potentially address the needs for bone tissue regeneration and provide an alternative, improved biomaterial for scaffolds.

III. Objectives

The objectives of this research are to characterize silk scaffolds in their ability to generate bone in critically sized femoral defects to be used in the treatment of bone disease and/or replacement. The specific goals are:

- To study silk as an alternative bone graft substitute to promote bone formation
- To analyze the osseointegration of different silk +/-cytokines +/- cells combinations with BMP-2 or RGD and hMSCs
- To identify the most suitable combinations of scaffold and scaffold decorations to optimize bone formation

IV. Materials and Methods

The overall goals of the project were to determine if a silk fibroin is a suitable scaffold biomaterial for osseous treatments. The preparation and fabrication methods of the silk fibroin are discussed in the following section. The specifications of how osseointegration was measured are described in detail.

7. *Materials*

Fetal bovine serum (FBS), RPMI 1640 medium, Dulbecco's Modified Eagle's Medium (DMEM), transforming growth factor- β 3 (TGF- β 3) were from R&D System in Minneapolis, MN. Basic fibroblast growth factor (BFGF) were from Life Technologies, Rockville, MD. Silkworm cocoons were supplied by M. Tsukada (Institute of Sericulture, Tsukuda, Japan) and Marion Goldsmith (University of Rhode Island, Cranston, RI). All other reagents were of analytical or pharmaceutical grade and obtained from Sigma (St. Louis, MO). BMP-2 was a gift from Wyeth Pharmaceuticals, Andover, MA (Thomas Porter). Hexafluoro-2-propanol (HFIP) and methanol were purchased from Aldrich.

8. *Silk Preparation*

The processing of the silk was done at Tufts University at the Medford campus, MA. The basic principles of this process are shown in Figure 5 (Kaplan, 2000). After receiving the silkworm cocoons from Japan, the worm was extracted and 3 cocoons were cut into 8 parts. The cocoons of *B. mori* silk were boiled for 1 hour in an aqueous solution of 0.02 Na₂CO₃ and 0.3% (w/v) Ivory soap solution. The silk was completely submerged at all times. Then the silk was rinsed with 1 L of hot unpurified tap water (UPW) and then 10 times with 1 L of cold UPW to

remove sericin proteins. The silk was dried overnight in a fume hood and the dry weight was measured.

The next day, the purified silk was dissolved in a 9 M LiBr solution at 55°C for 5 hours to give a 10% (w/v) solution of dried silk. The solution was filtered with a 5 µm syringe filter. 12 mL of the filtered solution was then inserted into a Slide-a-Lyzer dialysis cassette and dialyzed against 1 L of UPW. The UPW was changed after 1 hour, 3 hours, 6 hours, 9 hours and 12 hours. The dialyzed solution was pipetted into 25 ml aliquots in 50 ml Falcon tubes. It was then lyophilized and dissolved in hexafluoro-2-propanol (HFIP) to give a 2-3% (w/v) solution, which was determined by weighing the remaining solid after drying.

Films were formed by pipetting a volume of the solution onto the substrate (Falcon plates) to cover the surface area and then dried for 5 hours. Disk-shaped scaffolds (5mm diameter by 3mm thick) were prepared from the parent scaffold by using a dermal punch and autoclaved.

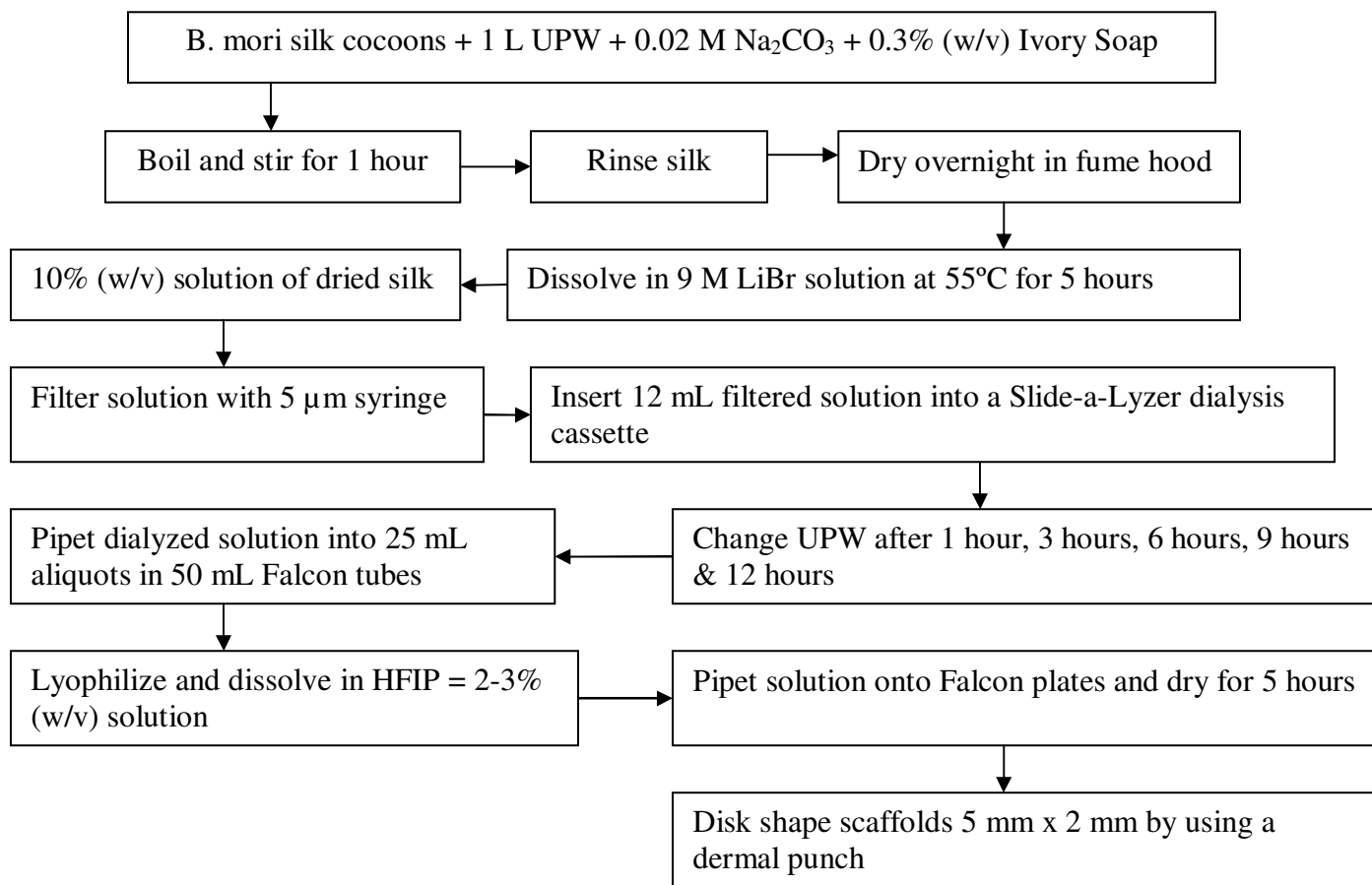


Figure 5: Methodology for Silk Scaffold Preparation (Unpublished data, 2005)

9. Silk Scaffold Fabrication

The fabrication technique utilized was salt leaching. A viscous solution was prepared by dissolving the silk in HFIP. Sodium particles acting as porogens were added to the plates and the silk/HFIP solution was then added (Unpublished data, 2005). In order to allow for homogenous distribution of the solution, the plates were covered to reduce evaporation rate. The solvent in the mixture of the silk/porogen composite was evaporated at room temperature. This composite was then immersed in methanol to induce β -sheet structure. The composites were then placed in water for 24 hours to ensure that all of the sodium particles had leached from the matrices. The fabrication process that follows the silk preparation is shown in Figure 6.

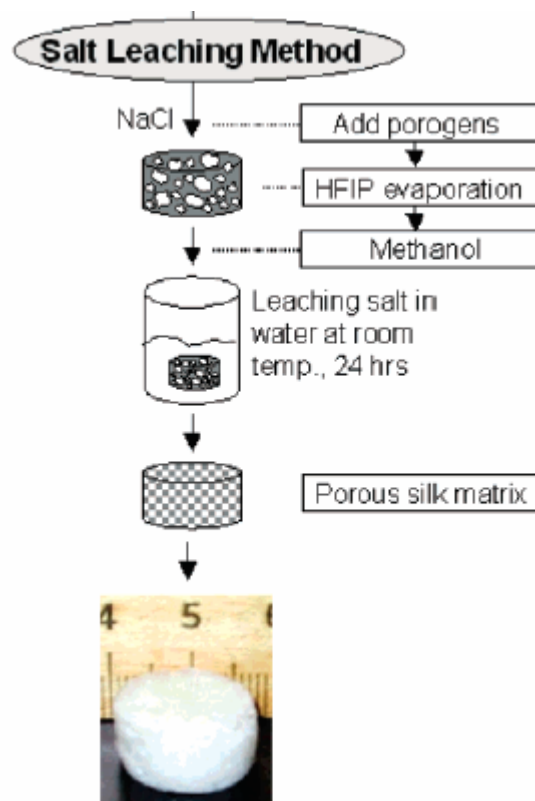


Figure 6: Silk scaffold fabrication flowchart with HFIP-derived silk *Adopted from Nazarov et al.

10. Modification of Silk by Covalent Coupling of Peptides

The silk films were modified, or decorated, with the following peptides: arginine-glycine-aspartic acid (RGD) peptides or BMP-2 by covalently bonding the amines on the peptide with the silk fibroin. The silk fibroin films that were cast after the addition of HFIP (as discussed above) were soaked in MES buffer (0.1 M MES, 0.5 M NaCl, pH 6) per dialysis cassette. This was done to hydrate the films and change surface arrangement by exposing hydrophilic functional groups. The MES buffer was changed the next morning. The fabrication technique used to form porous three-dimensional matrices was salt leaching.

The next evening the silk solution was carefully removed from the dialysis cassette and injected into a glass bottle with a syringe. 0.4 mg/mL of 1-ethyl-3-(dimethylaminopropyl)carbodiimide hydrochloride (EDC) and 1.1 mg/mL N-hydroxysuccinimide (NHS) were added to the solution and allowed them to react for 15 minutes at room temperature. These reagents activate the γ carboxyl (COOH) groups from aspartic and glutamic acids, which represent 2-3% of amino acids based on the amino acid composition of silk fibroin. The activated carboxyls are extremely reactive towards the primary amines on the peptides and form a stable covalent amide bond with the silk fibroin (Grabarek *et al.*, 1990).

Under a fume hood, 1.4 μ l of 2-mercaptoethanol per ml solution were added in order to quench the EDC. 7.5 mg of RGD or BMP-2 was then added to the reaction mixture and allowed the proteins to react at room temperature for 2 hours. The reaction was stopped by adding 10 mM of hydroxylamine HCl. This method hydrolyzes any unreacted NHS present on the silk's surface and results in the regeneration of the original carboxyls. Then 6-8 ml of the silk-RGD or silk-BMP-2 solution was inserted into a dialysis cassette and dialyzed against 1 L of UPW per

cassette. The UPW was changed after 1 hour, 3 hours, 6 hours, 9 hours and 12 hours. The dialyzed solution was pipetted into 25 ml aliquots in 50 ml Falcon tubes. The solution was frozen for 2 hours at -75°C . It was then lyophilized until it was completely dried, leaving a porous matrix, taking approximately 3 days. The silk films were subsequently treated with 90% methanol (v/v) to induce crystallization, induce a conformational change in silk to β -sheets, and to prevent resolubilization in the cell culture media (Asakura *et al.*, 1994). The lyophilized silk solution was then stored at room temperature. The basic methodology of this process is shown in Figure 7. This process starts off with the silk fibroin film that was cast after the addition of HFIP, as shown in Figure 5.

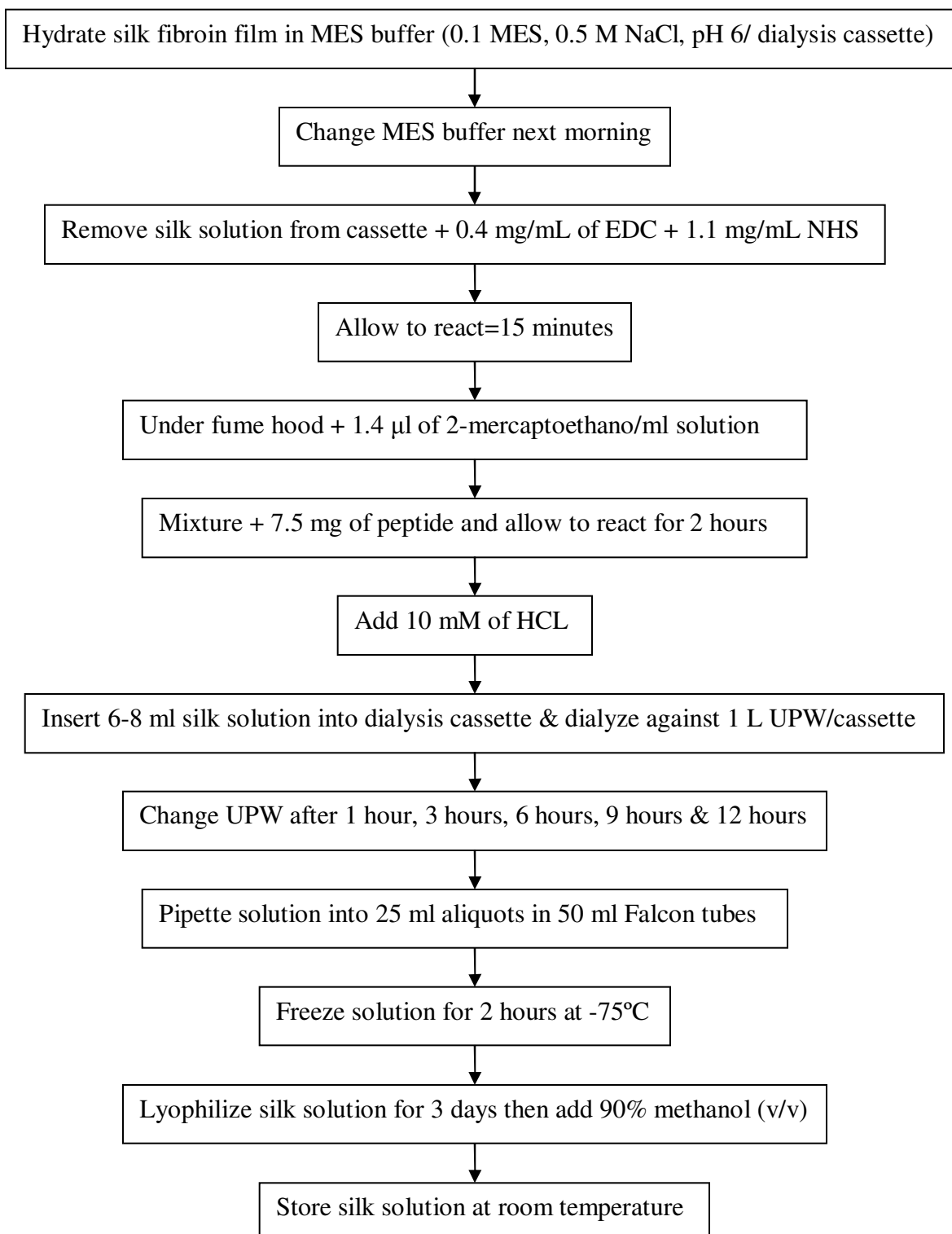


Figure 7: Process by which the silk was modified by covalent couplings of RGD peptides. Note: This process starts off with the silk fibroin film that was cast after the addition of HFIP, as shown in Figure 3.

11. *Human Mesenchymal Stem Cell Isolation and Expansion*

The hMSCs were isolated and expanded according to previous methods discussed (Meinel *et al.*, 2004). Whole human bone marrow (25 cm³ harvests) was obtained from Clonetics (Santa Rosa, CA) and was diluted in 100 mL of isolation medium (RPMI 1640 supplemented with 5% FBS). The hMSCs were isolated by density gradient centrifugation. The bone marrow suspension (20 mL aliquots) were overlaid on polysucrose (1.077g/mL, Histopaque, Sigma, St. Louis, MO) and centrifuged at 800 g for 30 minutes at room temperature. The cell layer that formed was removed and washed in 10 ml isolation medium, pelleted and the contaminated red blood cells were lysed in 5 ml of Pure-Gene lysis solution. The cells were then pelleted and suspended in a medium of DMEM supplemented with 10% FBM and 1 ng/ml bFGF and seeded in T75 flasks at a density of 5×10^3 cells/cm². 80% confluence was reached after 12-17 days for the first passage (P1). The cells were trypsinized, replated, and passaged for a second time (P2) reaching 80% confluence after 7 days. The P2 cells were used for the experiments (Meinel *et al.*, 2004).

12. *Operative Procedure*

Surgery was performed on one hind limb and the full length of the femur was exposed. A 5 mm critically sized defect was created in the rodents' femur. Silk implants were then placed into the defect. The specimens were administered the appropriate medication and observed on a daily basis over an eight week period.

12.1 Femoral Segmental Defect

Prior to the surgery, 8 male nude rats weighing 325-375 g were administered buprenorphine subcutaneously (0.05mg/kg) and procaine penicillin intramuscularly

(200,000IU/kg). They were labeled #69-76 and weighed before undergoing surgery. They were anesthetized with isoflurane (4-5%) and 1000 mL/min of O₂ and then transferred to the surgical table where anesthesia at 0.5-2% isoflurane and 600 mL/min of oxygen were administered through a nose cone face mask. Once the anesthesia was administered, the rat's respiratory rate and pattern were monitored every 5 -10 minutes throughout the surgery.

The anesthetized rat was positioned in left lateral recumbancy and one hind limb was prepared and draped in a sterile fashion. An approximately 25 mm long skin incision was made cranial to the femur and continued distally to the level of the lateral femoral condyle (Figure 8A). The subcutaneous tissue, fascia lata, and lateral fascia of the vastus muscle were carefully incised and separated. Retraction tools were used to pull the biceps femoris muscle posteriorly and the vastus muscle was retracted anteriorly. This exposed the full length of the femur (Figure 8B). An aluminum external fixation plate (15x4x4 mm) was placed over the lateral aspect of the femur and positioned appropriately in order to drill 4 holes in the bone, 2 in the proximal metaphysis and 2 in the distal metaphysis (Figure 8B). Once the drilling was complete, four 0.99 mm transverse-threaded Kirschner wires were extended 0.5 mm beyond the transcortex which was marked by a black line on the screws (Figure 8C, D, and E). Small incisions were made to the skin caudal to the 25 mm incision allowing it to be pulled over the Kirschner pins. The external fixator was then secured to the pins (Figure 8F). A 5 mm critical-sized full-thickness defect was created in the diaphysis with a 5 mm cutting burr while the area was irrigated with saline solution to remove bone debris as necessary (Figure 8F). The implants were then inserted into the defect (Figure 8G, H). Upon insertion, the muscle and subcutaneous tissues were sutured with a 4-0 Maxon suture. The skin was then closed separately with at 4-0 PDS II suture.

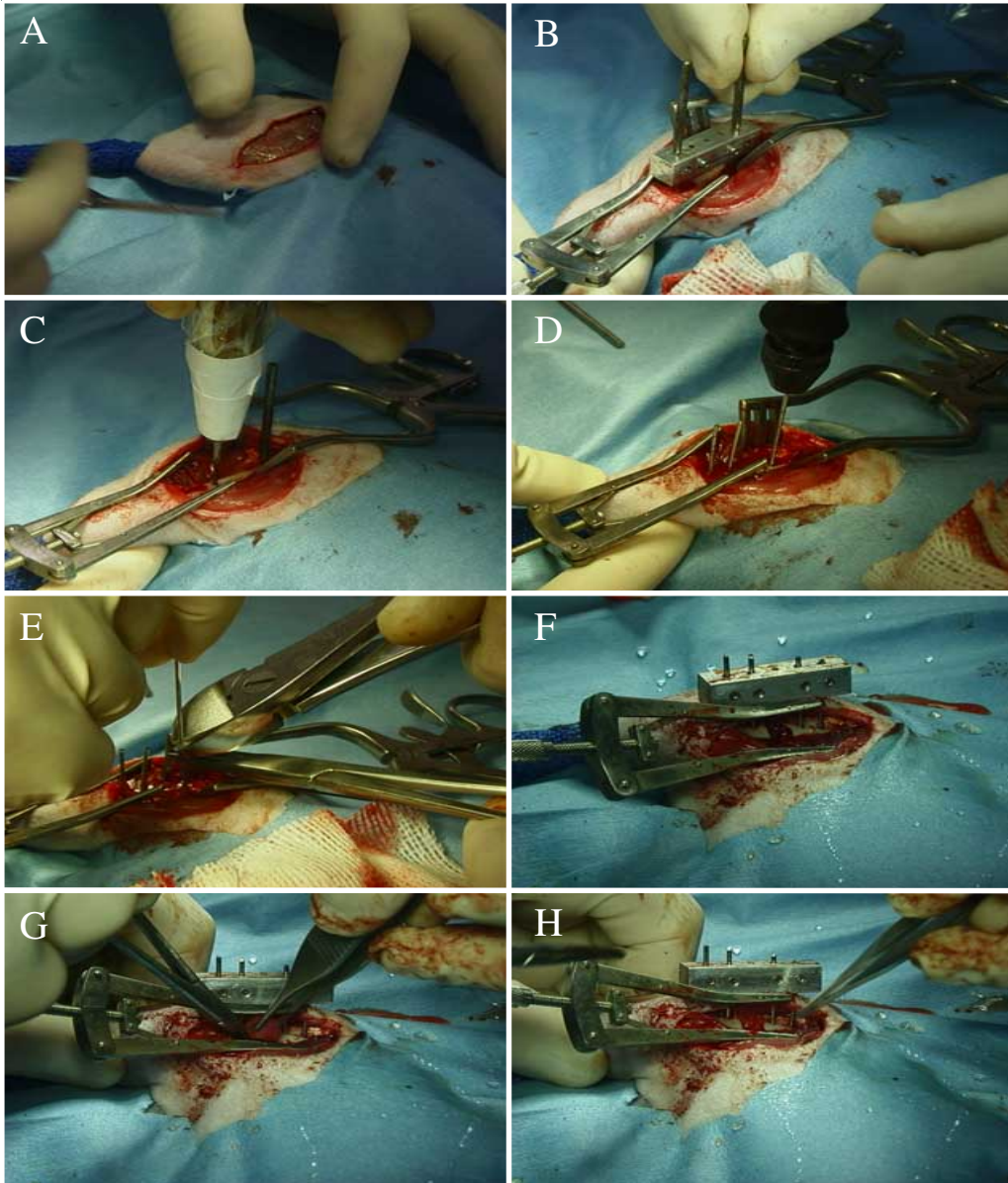


Figure 8: Surgical procedure for placing silk scaffolds in critical size femoral defects. A) skin incision, B) using fixator plate as a template for drilling, C) drilling pin hole, D) placing fixator pins, E) cutting pins, F) empty defect with fixator plate, G) placing implants into defect, H) defect with implants

Implanted in each femoral defect were two silk scaffolds placed longitudinally along the defect. A diagram of the external fixator and placement of the scaffolds are shown in Figure 9. The defects were filled with one of a series of different silk +/- cell +/- cytokine implant combinations that was based on the results of the heterotopic implantations (Table 12).

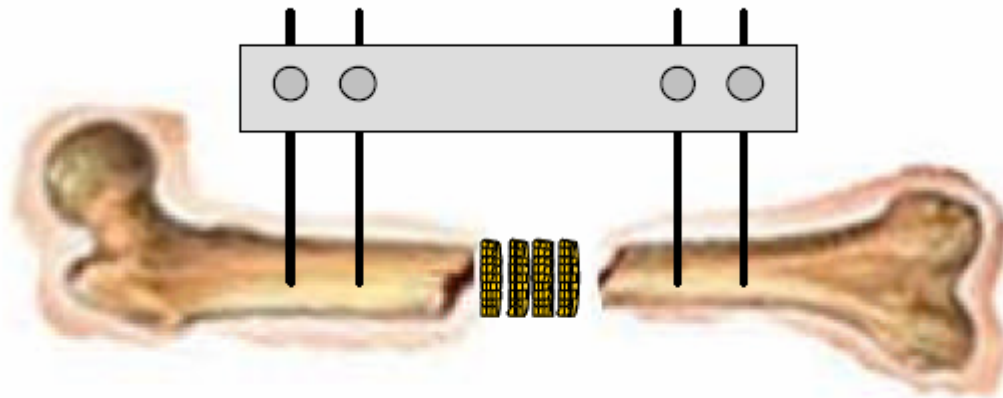


Figure 9: Critical size femoral defect fixed externally with a plate

Table 12: Scaffold Groups

Rat #	Treatment	Group#
69	Defects with tissue-engineered scaffolds covalently bound to RGD	3
70	Scaffolds with covalently bound RGD and undifferentiated hMSCs	4
71	Scaffolds with covalently bound RGD and undifferentiated hMSCs	4
72	Scaffolds with covalently bound RGD and undifferentiated hMSCs	4
73	BMP-2 loaded scaffold and undifferentiated hMSCs (seeded the day before the surgery)	7
74	Empty defect	1
75	Scaffolds with covalently bound RGD only	2
76	Scaffolds with covalently bound RGD only	2

12.2 Post-Operative Procedure

Immediately following surgery, the rats were administered 5 mg/kg of Carprofen subcutaneously. Each rat was wrapped in a paper towel and placed in a clean cage with heat provided by a heat lamp and monitored for cognizance every 15 minutes for 1 hour until the rat was ambulatory and cognizant of its environment. The rat was then administered 0.025 mg/kg

Buprenorphine subcutaneously 8 hours and 16 hours post-op. At 24 hours post-op, they were given 5 mg/kg of Carprofen and 0.025 mg/kg Buprenorphine subcutaneously and 200,000 IU/kg Procaine Penicillin intramuscularly. The weights of each animal were recorded. At 32 hours post-op, another 0.025 mg/kg of Buprenorphine was administered subcutaneously if the animal appeared to need it. At 48 hours post-op, the rats were given 5 mg/kg Carprofen subcutaneously and 200,000 IU/kg procaine penicillin intramuscularly. Each rat was then weighed again. Depending on the condition of each rat, additional doses of Carprofen were administered once every 24 hours and doses of Buprenorphine were administered every 12 hours if needed. If the rats need any additional doses of procaine penicillin, it was administered, but not more than a total of 4 doses.

Each rat was weighed twice a week until the study was complete. They were weighed more often if excessive weight loss was observed. As needed, the surgical wound was cleaned with chlorhexiderm and alcohol. Each rat was checked twice per day noting the following:

- Attitude and response to contact
- Changes in behavior, activity or posture,
- Pain or discomfort evidenced by twitching, falling over, back arching or lameness
- Observing the procedure area for redness, swelling, discharge or dehiscence
- Ensuring adequate daily food and/or water consumption

13. Scanning Electron Microscopy (SEM)

The segments of the silk scaffolds were fractured in liquid nitrogen (Kim *et al.*, 2004). The specimens were sputter coated with gold. The scaffold's morphologies and pore distributions, sizes and interconnectivity were observed with a LEO Gemini 982 Field Emission Gun SEM (Kim *et al.*, 2004). The pore sizes were determined by measuring random samples of 100 pores from the SEM images using ImageJ software developed at the US National Institutes of Health (Kim *et al.*, 2004).

14. Radiographs

Radiographs of the femoral defect were taken every two weeks to observe the progress of bone formation. The animals were sacrificed 8 weeks post-operation via carbon dioxide suffocation. The external fixator and implant remained in place following sacrifice. A qualitative evaluation from the X-rays was performed based on the bridging of the defect and the percentage of bone ingrowth following the qualitative measurements defined in Table 13. The evaluation from the X-rays was performed by 2 independent observers.

Table 13: Qualitative X-ray Measurements

Bridging of Defect Parameters	Percentage of Bone Ingrowth Parameters
Grade 1: trace radiodense material in the defect	Grade 1: minimal new bone composed of noncontiguous areas of minimal density
Grade 2: flocculent radiodensity with flecks of calcification and incomplete bridging of the defect	Grade 2: new bone present as mostly contiguous areas of normal density and filling <50% of defect
Grade 3: bridging of the defect in at least one location with material of non-uniform radiodensity	Grade 3: new bone present as mostly contiguous areas of normal density and fills 51-95% of the defect
Grade 4: bridging of the defect at both the cis and trans cortex with material uniform radiodensity, cut ends of cortex remain visible	Grade 4: new bone a solid contiguous mass that fills >95% of the defect
Grade 5: obscuring of at least one of the two cortices by new bone	
Grade 6: bridging of the defect by uniform new bone, cut ends of cortex not seen	

15. Dual Energy X-ray Absorptiometry (DEXA) Scanning

Following euthanasia after eight weeks post-operative, the femurs were scanned using a Hologic QDR 1000W with the regional high resolution scan mode. The external fixators and k-wires remained in the femur. A general, or global, region of interest was selected to include the area of the defect in addition to the proximal and distal portions of the femur. The k-wires were not included in the selected area. There were three subregions selected to only include the defect area. Region 1 was a small area the same size as the defect. Region 2 was approximately 5 mm in height with a length three times the width of the defect. This would provide a means to include any bone or callous formation that occurred beyond the defect region. Region 3 was the same length as region 2, however it was half of the height. This placed it directly in the center of the defect.

Each specimen was scanned twice with a third scan taken if the scans varied more than 5%. In this case, the two closest were averaged to obtain the values. The values determined from the DEXA scans were bone area (cm^2), bone content (g), and bone mineral density (g/cm^2). The obtained values for regions 1-3 and the global values can be found in Appendix C.

In order to have control values to compare the defect data with, scans were taken of the healthy femur on the opposite leg. This was done in the same manner as described above. A global region and regions 1-3 were acquired and these values can be found in Appendix D. Similarly, the values that were obtained were bone area (cm^2), bone content (g), and bone mineral density (g/cm^2).

V. Experimental Design

This section explains the rationale behind the processes that led up to a final silk matrix. These include matrix fabrication, control of the architecture, and decoration. Such controls were analyzed using SEM, DEXA, and radiographs.

16. Matrix Preparation

Based on data gathered in a previous study conducted at Tufts University, a salt leaching method was adopted in the experiment. The research analyzed three methods of scaffold preparation for silk based on their prior use in processing of other types of polymers (Nazarov, 2003). These included freeze-drying, salt leaching, and gas foaming. The most promising methods were determined by comparing the mechanical properties (compressive resistance) and porosities.

For the freeze-drying method, the scaffolds that formed were highly interconnected and porous however the pore sizes were very small (Nazarov, 2003). The porosities were 99% regardless of the variables studied (Table 14). The pores were larger with the salt leaching method (202) in comparison to the freeze-drying method. The pore structure, however, was not as highly interconnected. NaCl was used as a porogen in this method and was leached out in water to form the porous matrix (Nazarov, 2003). Scanning Electron Microscopy (SEM) images showed that the gas foaming method also had a highly interconnected pore structures compared to salt leaching (Figure 10) with pore sizes around 155 (Nazarov, 2003). However, as the porosity increased the scaffolds were not as strong and flaked apart. The salt leaching and the gas foaming methods had varying porosities as the porogen-to-silk ration was varied (Table 14) (Nazarov, 2003). The complete data are shown in Table 14. The mechanical data that was collected can be found in Table 15.

Table 14: Porosity and Density of the Scaffolds (Average \pm S.D., N=3) for Porosity and Density Measures (for Pore Sizes, N= 200)

Methods	Sample	E (%) ^a	Density (mg/mL)	Pore Size
Gas foaming	NH ₄ HCO ₃ /silk (wt %)			
	10:1	87.0 \pm 2.0	100 \pm 10	155 \pm 114
Salt leaching	NaCl/silk (wt %)			
	10:1	84.0 \pm 2.0	120 \pm 2	202 \pm 112
Freeze-drying (frozen at -20°C) (frozen at -80°C)	20:1	98.0 \pm 1.0	40 \pm 5	
	alcohol treatment ^b			
	15% methanol	98.0 \pm 0.10	20 \pm 2	
	25% methanol	99.0 \pm 0.01	30 \pm 1	50 \pm 20
	15% propanol	98.0 \pm 0.01	30 \pm 3	
	25% propanol	99.0 \pm 0.20	30 \pm 3	
	15% methanol	99.0 \pm 0.30	50 \pm 3	
	25% methanol	99.0 \pm 0.03	40 \pm 1	15 \pm 7
	15% propanol	97.0 \pm 0.20	30 \pm 3	
	25% propanol	99.0 \pm 0.02	30 \pm 5	

^a Porosity. ^b Weight ratio of water in alcohol. *Adopted from Nazarov et al.

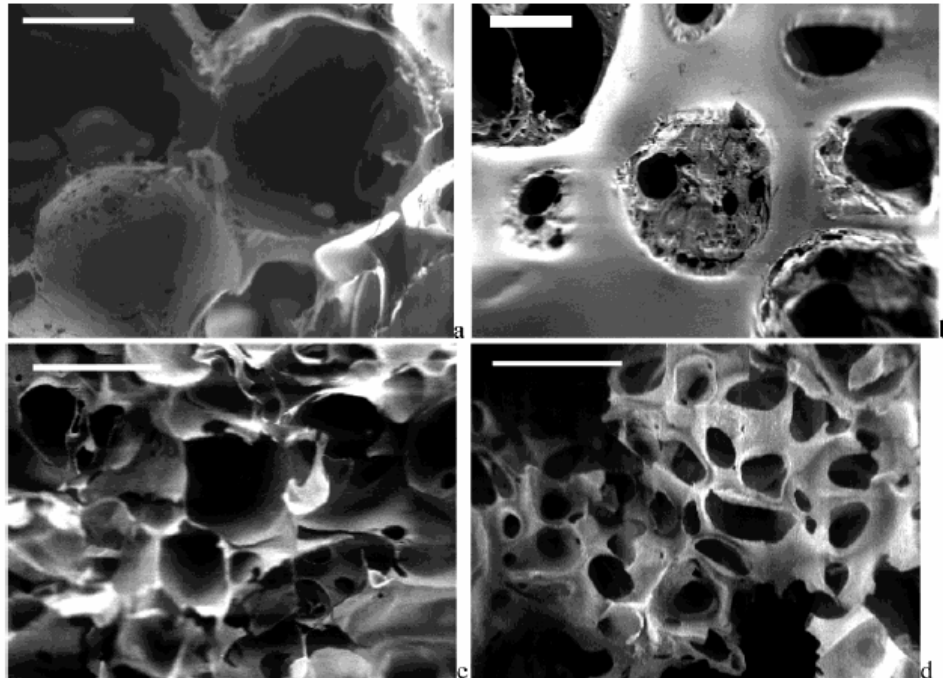


Figure 10: SEM images of the inner and outer structure of the silk scaffold by salt leaching and gas foaming after methanol treatment (scale bar: 200 μ m) a.) NaCl:silk (10:1 wt%) (inner) b.) NaCl:silk (10:1 wt%) (outer) c.) NH₄HCO₃:silk (10:1 wt%) (inner) d.) NH₄HCO₃:silk (10:1 wt%) (outer) *Adopted from Nazarov et al.

Table 15: Compressive Stress and Modulus of the Silk Scaffolds

Method	Sample	Alcohol Treatment ^a	Compressive Stress (kPa)	Compressive Modulus (kPa)	
gas foaming	NH ₄ HCO ₃ /silk (wt %) 10:1	methanol	280 ± 4	900 ± 94	
		1-butanol	230 ± 9	500 ± 37	
		2-propanol	250 ± 28	800 ± 44	
	20:1	methanol	250 ± 21	1000 ± 75	
		1-butanol	150 ± 8	300 ± 40	
		2-propanol	100 ± 11	200 ± 30	
salt leaching	NaCl/silk (wt %) 10:1	methanol	30 ± 10	100 ± 2	
		1-butanol	150 ± 14	400 ± 50	
		2-propanol	100 ± 20	400 ± 58	
	20:1	methanol	175 ± 3	450 ± 94	
		1-butanol	250 ± 4	490 ± 94	
		2-propanol	200 ± 3	790 ± 3	
freeze-drying	freeze temperature	none	80 ± 1	170 ± 7	
		15% methanol	10 ± 2	20 ± 1	
		25% methanol	10 ± 3	10 ± 3	
		15% 2-propanol	10 ± 2	40 ± 4	
		25% 2-propanol	10 ± 3	50 ± 8	
		none	20 ± 2	220 ± 7	
	-20 °C	15% methanol	20 ± 3	90 ± 21	
		25% 2-propanol	5 ± 4	90 ± 40	
		15% methanol	30 ± 2	100 ± 1	
		25% 2-propanol	20 ± 1	130 ± 1	
		-80 °C	15% methanol	30 ± 2	100 ± 1
			25% 2-propanol	20 ± 1	130 ± 1

^a 100% unless otherwise indicated, weight percent of the alcohol in water. *Adopted from Nazarov, *et al.*

Table 16: Average Compressive Strength and Average Compressive Modulus of Gas Foamed and Salt Leached Scaffold at 1% and 2% Strain under Compressive Load (N=2)

Scaffold	Porogen Ratio	Average Compressive Modulus (KPa) at 1% strain	Average Compressive Strength (KPa) at 1% strain	Average Compressive Modulus (KPa) at 2% Strain	Average Compressive Modulus (KPa) at 2% Strain
Salt leached	10:1	40	0.40	400	8
	20:1	1600	16	1200	24
Gas formed	10:1	500	5	200	16
	20:1	5000	50	3000	60

*Adopted from Nazarov, *et al.*

The gas foamed scaffolds reached a definitive compressive yield point where the scaffold was permanently deformed. However, the salt leached scaffolds demonstrated characteristics that were more ductile and sponge-like in behavior (Nazarov *et al.*, 2003). Table 15 shows that the gas foamed scaffolds had a higher compressive strength and compressive modulus than the salt leached scaffolds. However, both of the methods were comparable in terms of mechanical properties with other polymeric biomaterial scaffolds used in bone tissue engineering (Nazarov *et al.*, 2003). In bone related engineering applications, matrices are designed to hold a load allowing for 1-2% strain. The gas foamed and salt leached scaffolds prepared with methanol were analyzed as a load is applied (Table 16). Of the scaffolds prepared, these groups were determined to be the most likely used in bone engineering applications (Nazarov *et al.*, 2003).

Although the scaffolds formed by gas foaming had higher compressive properties and porosity based on the above study, the salt leaching method was adopted in the present experiment. The characteristics shown from the salt leaching method meet the requirements related to bone tissue engineering. Additionally, after speaking with Dr. Kaplan and Dr. Kirker-Head of Tufts University, it was established that the salt leaching method would suffice for the experiment.

Methanol is used in order to induce a conformational change in the silk (silk I) to the crystalline β -sheet structure (Nazarov *et al.*, 2003). When methanol is immersed in the silk solutions, water is removed from the hydrated hydrophobic domains and increases chain-chain contact and formation of β -sheet structures. Other alcohols, such as 2-propanol, are less hydrophilic and therefore are less miscible with water (Nazarov *et al.*, 2003). When immersed in the silk solution, less dehydration occurs and fewer β -sheet structures are induced when compared to methanol treated scaffolds. In the present experiment 90% methanol is used to

induce transformation (Nazarov *et al.*, 2003). Studies have shown that with an increase in the concentration of methanol, the compressive modulus is also increased. This is due to the increase in crystallinity of the silk after introducing the methanol. Additionally, at a higher concentration, the chain rearrangements are more rapid and extensive and lead to an increase in β -sheet content (Nazarov *et al.*, 2003).

The pore size and the porosity of the scaffolds were regulated by the addition of granular NaCl with particle sizes ranging from 100-1000 μm in diameter. In this process, most of the salt particles were retained in the scaffold while the surface of the salt dissolved in the fibroin solution. Previous studies observed that the solubility of the silk protein decreased when NaCl concentration was increased (Kim *et al.*, 2004). With a higher salt concentration, more water molecules are needed to hydrate the ions. As a result, the water molecules are easily removed from the fibrous proteins and interactions among the proteins becomes favored. This provides for a more stable structure and the induced chain-chain interactions result in β -sheet formation (Kim *et al.*, 2004).

17. Characterization of Matrix

The silk scaffolds were characterized by Scanning Electron Microscopy (SEM) to determine the porosities and homogeneity in structure (Unpublished data, 2005). The pore size was calculated from means with at least 100 pores determined by image analysis and the values were reported as a means \pm standard deviation (Unpublished data, 2005). This analysis was conducted before any peptides or cells were incorporated into the scaffold. Similar analyses were also conducted after cell and bone growth to determine any changes in the structure and the distribution of the changes (Unpublished data, 2005). This technique is routine in the labs at Tufts University.

18. Peptide Coupling

Another objective in designing the experiment was to assess the role of cell signaling factors immobilized on silk as a biomaterial template. Preliminary tests were conducted with different combinations and concentrations of different signaling factors (Unpublished data, 2005). These included GRGDS containing the adhesion ligand RGD, GRYDS (control), the first 34 amino acids of parathyroid hormone (PTH1-34) and a modified version of PTH1-34. Each of the following signaling factors is related to the induction of bone formation. The GRGDS peptide was selected on the basis of being well-documented and the interaction between the GRGDS sequence found in fibronectin and integrins (Unpublished data, 2005). GRYDS is used as a control sequence in order to compare to RGD. Preliminary studies were conducted to clarify the role of the control RYD versus RGD and PTH 1-34 versus the modified PTH 1-34 and also to use the information found in the next phase of the study (Unpublished data, 2005).

In preliminary studies, the adhesion of human osteoblast like cells were analyzed after 4 hours of attachment to the substrates in the presence of 1% and 10% serum or no serum (Unpublished data, 2005). In serum free cultures, significantly more cells adhered to the RGD/silk, PTH/silk substrates than to silk alone. The adhesion of the cells to the control substrates was comparable to that of silk (Unpublished data, 2005). Similar results were found when bovine mesenchymal stromal cells were incorporated into the scaffolds (Figure 11).

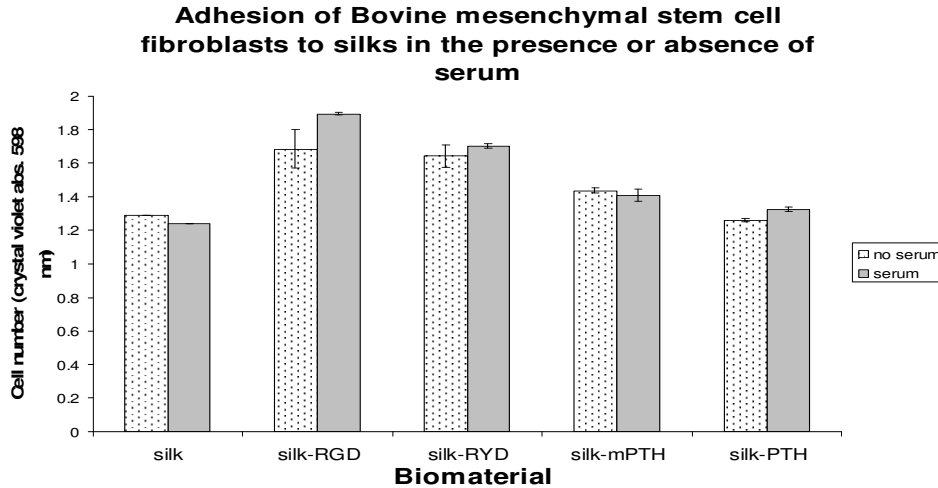


Figure 11: Adhesion of bovine mesenchymal stem cell fibroblasts to silk substrates in the presence or absence of serum *Adopted from Sofia *et al.*, 2000

The number and size of the nodules found in the culture were also determined (Unpublished data, 2005). According to the work of Bellows *et al.*, if numerous nodules are found in the culture, it provides a rough estimate of the osteoprogenitor cells present that are capable of proliferating and differentiating (Bellows *et al.*, 1989). If there are few large nodules present, it can be presumed that there are fewer osteoprogenitor cells, but the osteoblasts present in the nodule are rapidly differentiating and increasing mineralization of the matrix (Bellows *et al.*, 1989).

The number of nodules determined on each substrate is found in Figure 12A (Sofia *et al.*, 2000). By 4 weeks of culture, there were no significant changes observed except with RGD/silk substrate with a 25% increase in the number of nodules. This suggests that the number of osteoprogenitors is rapidly increasing on this substrate (Sofia *et al.*, 2000). It was also found that nodule area increased on the RGD substrate, insinuating increased osteoblast differentiation (Figure 12B) (Sofia *et al.*, 2000). The response of the osteoblasts to the decorated silk supports silk as a suitable bone-inducing matrix. The results confirm that this is particularly true for the RGD/silk substrates, but not for either PTH substrate (Sofia *et al.*, 2000). This provided a means

to narrow the choices for the type of surface modification used. The next phase focused only on the peptide RGD and the growth factor BMP-2 (Sofia *et al.*, 2000). Because the PTH substrates did not prove to serve as suitable matrices, another peptide related to bone formation was studied (BMP-2). BMP2-7 plays an active role in bone development and growth where BMP-2 was used in the following experiments because it was graciously donated by Wyeth Pharmaceuticals.

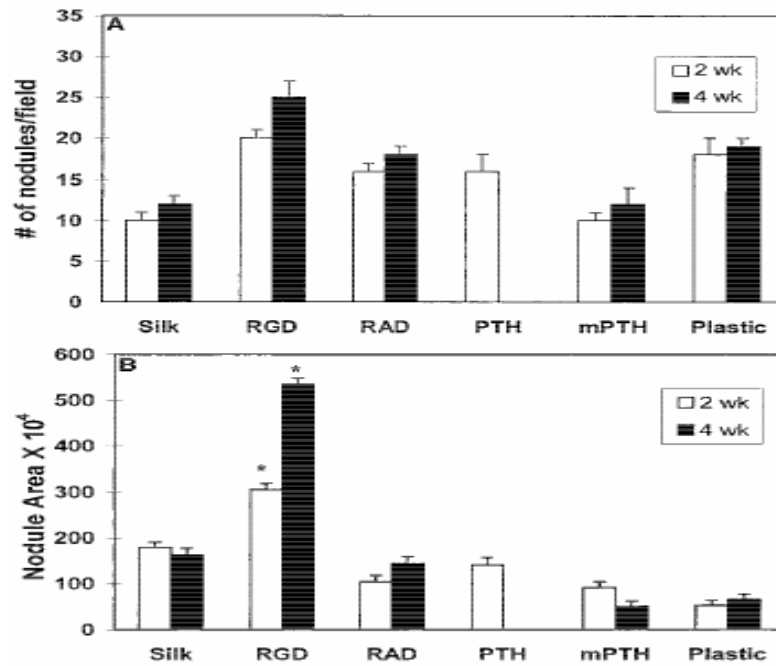


Figure 12: (A) Nodule numbers and (B) areas formed by the Saos-2 osteoblast-like, human osteoblasts grown on the various silk films at 2 and 4 weeks. *= $p < 0.05$ compared to control (silk). **Adopted from Sofia *et al.*, 2000

19. Model System

Living animals are required for this study due to the complexity of the processes being evaluated and therefore were unable to be duplicated or modeled in simpler systems (Unpublished data, 2005). Additionally, there is little known about bone morphogenesis and repair processes that would allow an appropriate nonliving model. In addition, preclinical studies in living animals are necessary prior to human testing (Unpublished data, 2005).

Since these investigations are evaluating a novel material and there has not been extensive research before this point, a rodent model is typical. Once it is demonstrated that silk is a promising material for orthopedic applications, the animal model system can progress to larger animals with a similar bone physiology to humans (Unpublished data, 2005).

Rats are a well established model for testing osteoinductive materials when combined with carrier substrates (Unpublished data, 2005). Therefore, the animal model system of choice was the nude rat. Rats are financially feasible in comparison to larger animals. The use of nude rats also allows the use of non-rodent cell types because they lack an immune response and therefore will not reject human mesenchymal stem cells upon implantation (Unpublished data, 2005). This species has been selected because a large database exists which would allow comparisons with previous data. Nude rats are also the phylogenetically lowest species that provides adequate size, tissue, and anatomy for the proposed study (Unpublished data, 2005). Additionally, the background of this project was established in previous studies at Tufts using the nude rat species.

The number of rats required for the study of silk as a scaffold for bone tissue regeneration is 328 over a period of three years. During this time, it is intended to complete 66 heterotopic implantations. To date, Tufts has used 35 rats for this study. This total will provide approximately 100 combinations of silk +/- cytokine +/- cells. Additionally, there have been 37 out of 200 rats approved for this phase of the study, which is assessing orthotopic bone formation *in vivo* in critically-sized femoral defects. This enables up to 40 combinations of silk +/- cytokine +/- cells in these defects to be tested.

20. Assessment of in vivo Bone Formation

In order to determine the osteogenic potential of the silk scaffolds post-implantation, plain radiographs were taken at 0, 2, 4, 6, and 8 week intervals. This method provides a means to qualitatively determine whether or not bone formation has occurred. It provides a means to visually account for density changes. In order to obtain quantitative data to better understand how the scaffold combinations affected bone ingrowth, DEXA analyses were performed post mortem. These forms of analyses were suggested by Dr. Kaplan and Dr. Kirker-Head from Tufts University. They were also performed in the preliminary studies and therefore to maintain consistency in evaluating results, the preceding methods were adopted in this phase of the experiment.

VI. Results

21. X-ray Evaluation

The defects with the RGD covalently bound to scaffolds with TE hMSCs (Rat 69) and one rat in the RGD and undifferentiated hMSCs (rat 72) showed trace radiodense material (Figure 13A) and minimal new bone (Figure 13B) for all time points. There was minimal bone ingrowth for Rat 71 (RGD and scaffold with undifferentiated hMSCs), and Rat 75 and 76 (RGD scaffold only) for all time points. The addition of hMSCs (both undifferentiated and TE) to the scaffolds with covalently bound RGD did not induce bridging of the defect or percentage of bone ingrowth. The results were comparable to that of the RGD covalently bound to scaffolds only.

Healing was evident in the X-rays for Rat 73. The scaffolds loaded with BMP-2 showed bridging of the defect in at least one location with material of non-uniform radiodensity. Bone ingrowth of normal density and filling was present in less than 50% of the defect (Figure 13B). Both occurred in the sixth week post-operative. Results comparing the addition of undifferentiated versus tissue engineered hMSCs could not be made since only BMP-2 loaded scaffolds with undifferentiated hMSCs were used in this experiment.

These results show that the BMP-2 loaded scaffolds with undifferentiated hMSCs and the empty defect induced bridging of the defect and bone ingrowth. Although the latter obscured the most of the two cut cortices and formed new bone in more than 50% of the defect, the results were unexpected.

It should be noted that results are not available for rat #70. It was a member of the treatment group with RGD covalently bound to the scaffolds with undifferentiated hMSCs. The death occurred two days post-surgery and was possibly the result of a reaction to the injections.

The death of the rat does not have an impact on the results obtained since there were still two other rats in the same treatment group in this phase of the experiment.

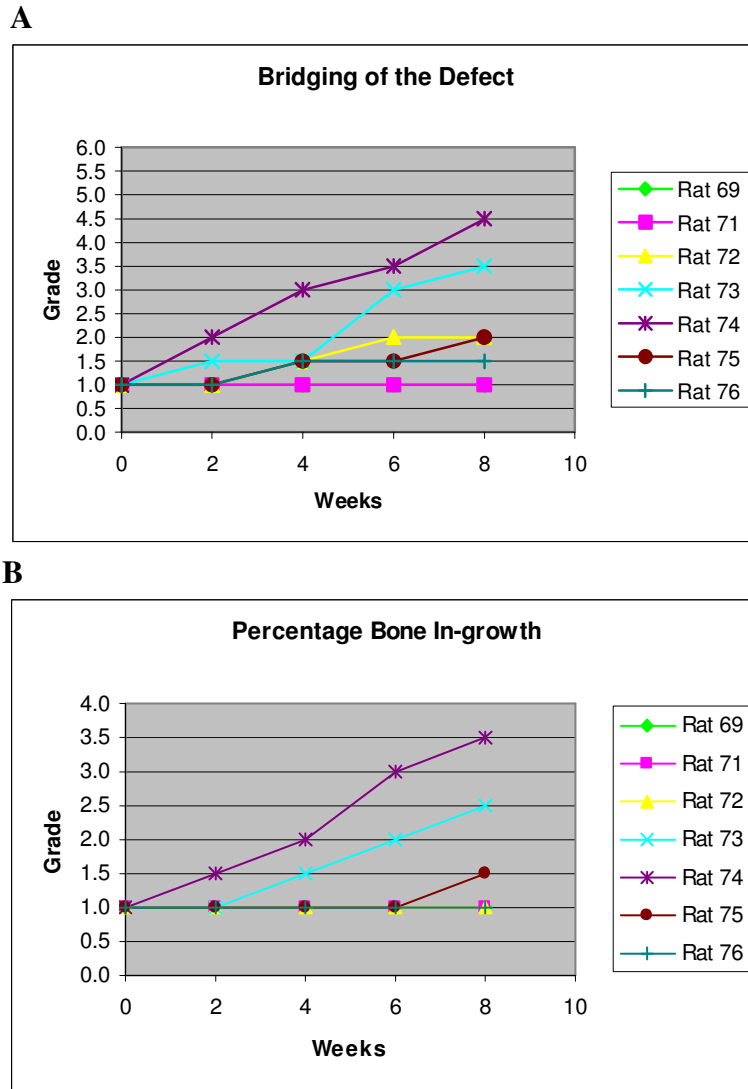
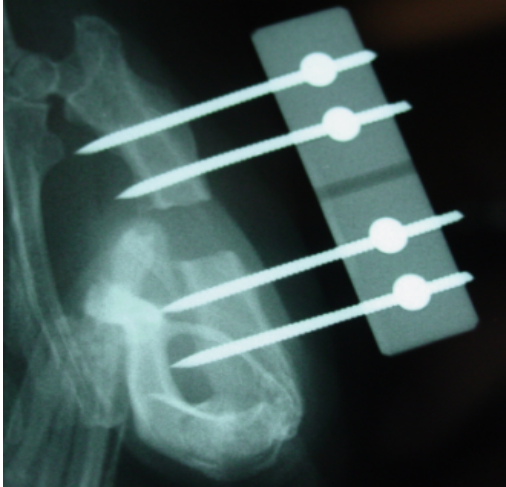


Figure 13: Qualitative analyses for bridging of the defect and percentage of bone ingrowth are shown in graphs A and B respectively. This scoring was done for defects with RGD covalently bound to scaffolds with tissue-engineered hMSCs (Rat 69), defects with RGD covalently bound to scaffolds with undifferentiated hMSCs (Rat 71 and Rat 72), defects with BMP-2 loaded scaffolds with undifferentiated hMSCs (Rat 73), empty defects (Rat 74), and defects with RGD covalently bound to scaffolds only (Rat 75 and Rat 76).

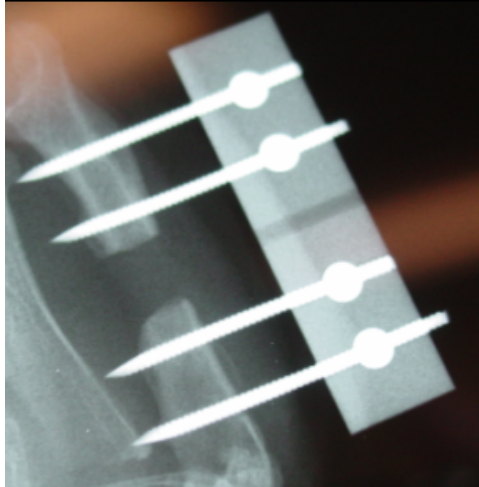
The final X-rays from the different rats are presented in Figure 14. All of the radiographs taken at each time period can be found in Appendix B. There is minimal healing in A, B, C, F,

and G. It should be noted that the below X-rays demonstrate that the most activity is occurring in E which is counterintuitive considering that it is the empty defect.

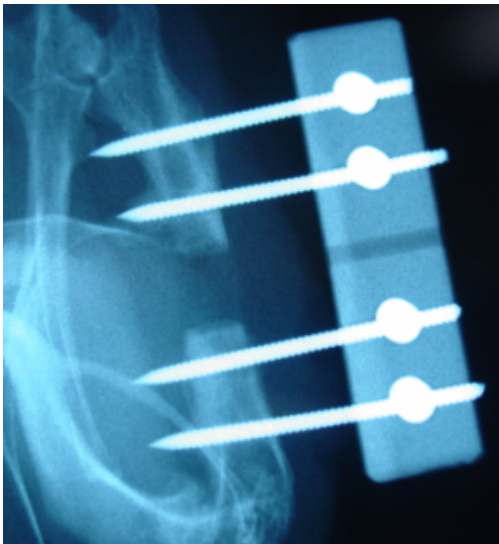
A



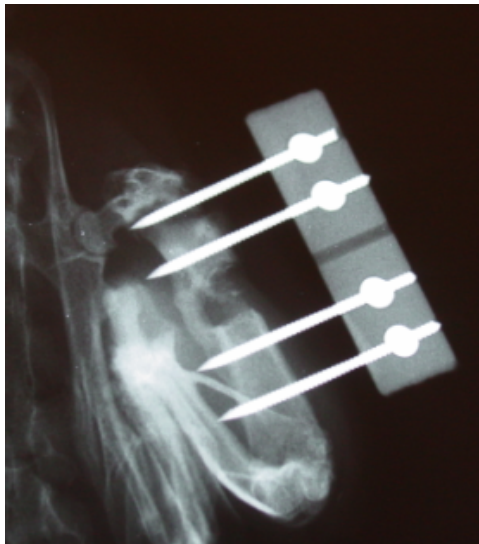
B



C



D



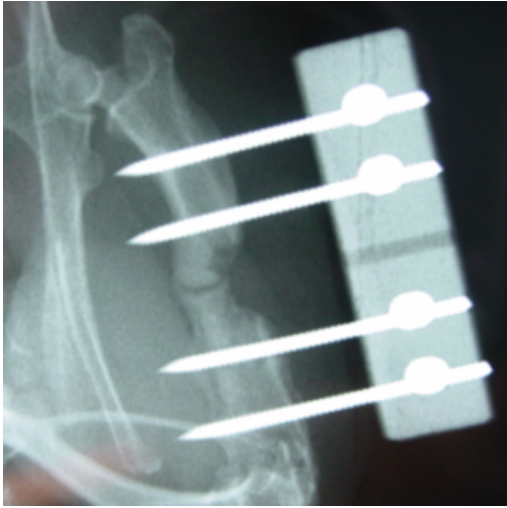
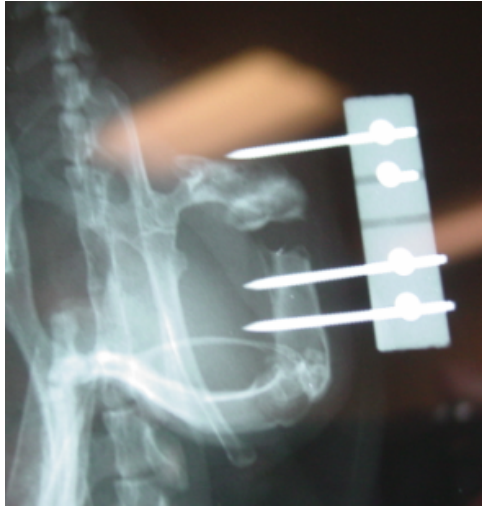
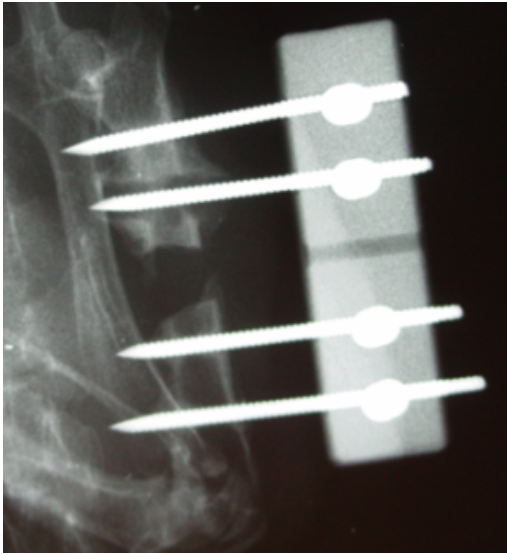
E**F****G**

Figure 14: X-rays that were taken of the femoral defect of Rat 69 (A), Rat 71 (B), Rat 72 (C), Rat 73 (D), Rat 74 (E), Rat 75 (F), and Rat 76 (G).

22. DEXA scanning

The results obtained from qualitative scoring of the X-rays were compared with DEXA scanning after the rats were euthanized (Figure 15). The values that were obtained for bone area, content, and mineral density for the defected area can be found in Appendix C. In general, rats 69, 71, and 72, which had the scaffolds with covalently bound RGD with hMSCs, showed the least bone ingrowth (Figure 15). However, the density for Rat 72 was higher than for Rat 71 even though they are both in the same group (RGD and undifferentiated hMSCs).

The density of the new bone was highest for rat #75 (0.2121 g/cm^2) with the RGD scaffold implanted in the defect. However, Rats 73, 74, & 75 did not show a significant difference in the area, mineral content, and mineral density of the newly formed bone. Rat 76 had similar mineral density, area and content values to Rat 72 and 69 (Figure 15).

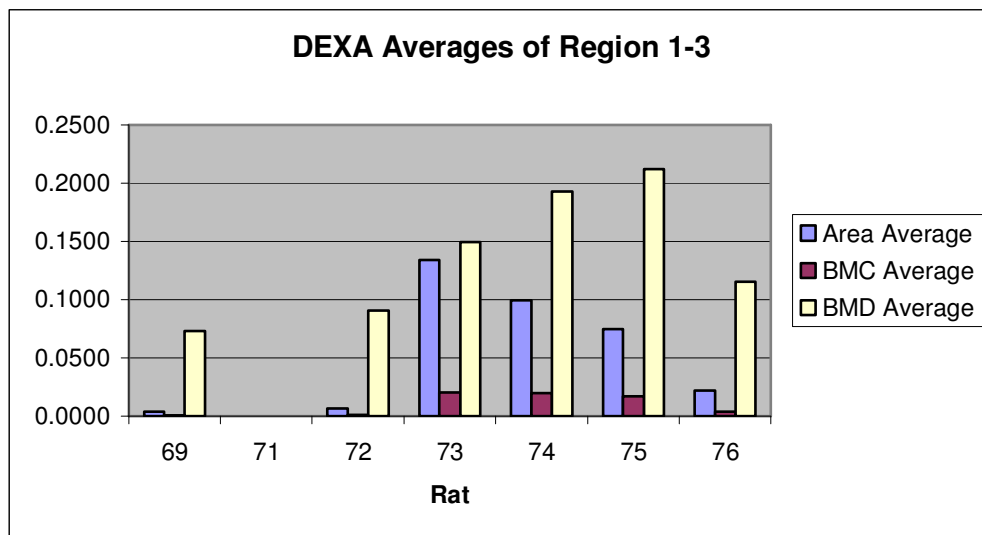


Figure 15: DEXA scanning of femoral defect with implants for mineral density (g/cm^2), area (cm^2), and bone content (g). The data is from each rat: RGD covalently bound to scaffolds with tissue-engineered hMSCs (Rat 69), RGD covalently bound to scaffolds with undifferentiated hMSCs (Rat 71 and Rat 72), BMP-2 loaded scaffolds with undifferentiated hMSCs (Rat 73), empty defects (Rat 74), and RGD covalently bound to scaffolds only (Rat 75 and Rat 76).

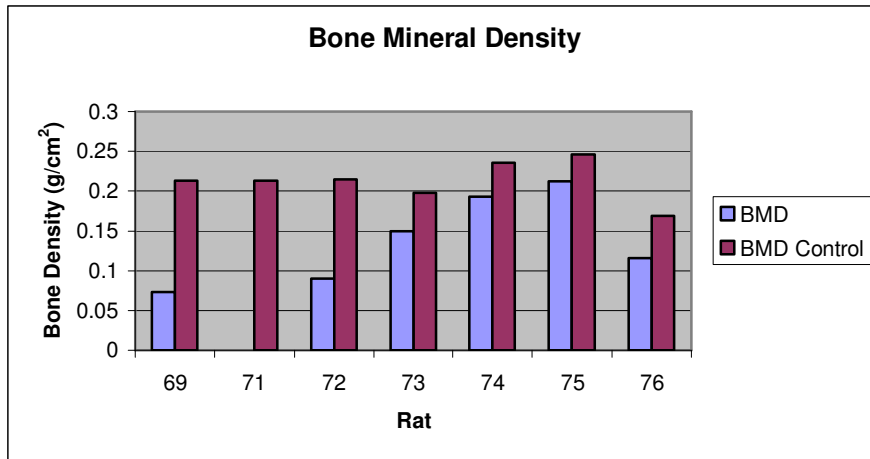
The average values for Regions 1-3 were also compared to control values for bone mineral content, area, and density that were obtained from analysis of the healthy, unaffected femur (Figure 16A-C). The bone content and area values remained extremely small (if not zero) compared to the control values for rats 69, 71, and 72 (of which, 71 and 72 are in the same group), the bone density was closer to the control for rat #72. The control bone density value was 58% higher than the recorded DEXA value. Rat #72 also had slightly increased values for bridging of the defect scoring compared to rat #71 (Figure 13A). The radiographs also corroborate the DEXA in regards to Rat 69. The X-rays showed trace radiodense material and minimal bone ingrowth and according to Figure 15, Rat 69 has the smallest bone density value compared to the other specimens.

The bone mineral density values for Rats 73, 74, and 75 are closest to their corresponding control density values. The control bone density values were 25%, 18%, and 14% higher than the recorded values for Rats 73, 74, and 75 respectively (Figure 16A). The qualitative analysis confirms this for Rats 73 and 74. However, there is little bone growth activity occurring in the defected area of Rat 75 according to Figure 13. In the X-ray evaluation, rats 75 and 76 showed new bone area and content comparable to rats 71 and 72. Both of the groups (rats 75 & 76 members of group 2 and rats 71 & 72 members of group 4) displayed minimal new bone and bridging in the X-rays (Figure 14B, C, F, and G). Therefore, the qualitative analysis for Rat 75 is not corroborated by the DEXA analysis.

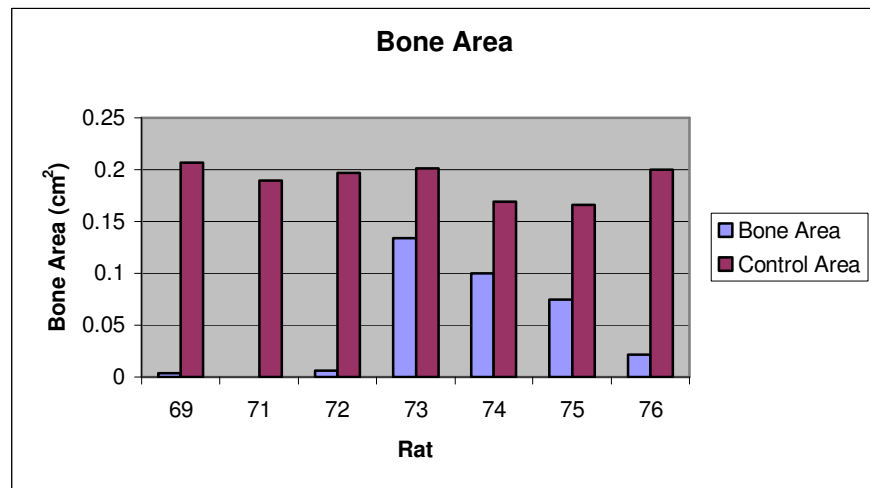
Rats 73, 74, and 75 also shows high bone mineral content and area within a decent range to the control values in comparison to the other rodents. For rat 73, the control values were 33% higher compared to the defected bone area value, and 48% higher compared to content. Similarly, for rat 74, the control values were 51% and 41% higher than the values recorded

within the defect for bone content and area respectively (Figure 16A, B). This, however, is corroborated by the qualitative evaluation (Figure 13A & B). The control values were 59% and 55% higher than the defected values for content and area respectively for rat 75.

A



B



C

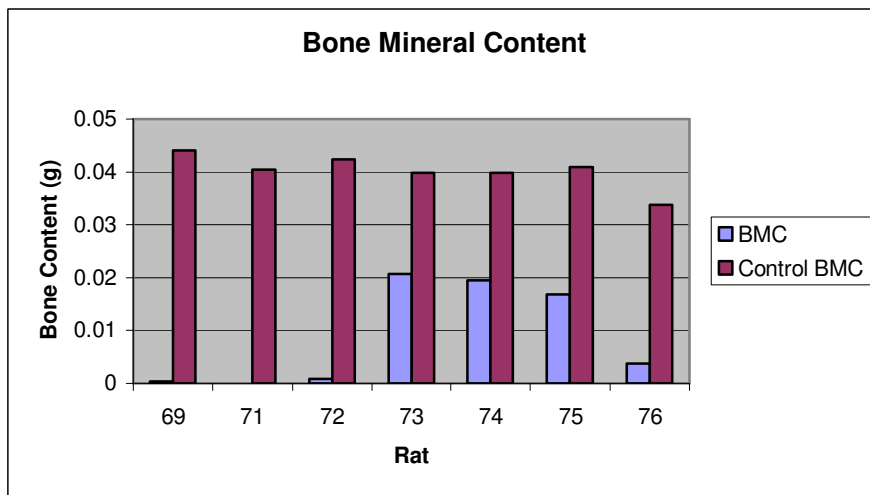


Figure 16: The average DEXA values (Regions 1-3) were compared to control values of the healthy, opposite hind limb of the rodents (A) Bone mineral density values were compared to control density values (B) Bone area values were compared to control area values (C) Bone mineral content values were compared to control content values²²

22. Morphology

The HFIP-derived scaffolds are characterized by a highly interconnected network of pores and smooth surfaces (Figure 17). The pore sizes had an average diameter of $890\pm 50\ \mu\text{m}$. In preliminary studies with HFIP silk scaffolds, the pore sizes followed a Gaussian distribution due to the NaCl porogens not being sieved. Passage 2 hMSCs were seeded onto the HFIP-derived silk and were analyzed after 1, 14, and 28 days. SEM analysis demonstrated that the distribution of the hMSCs was non-uniform (Figure 17).

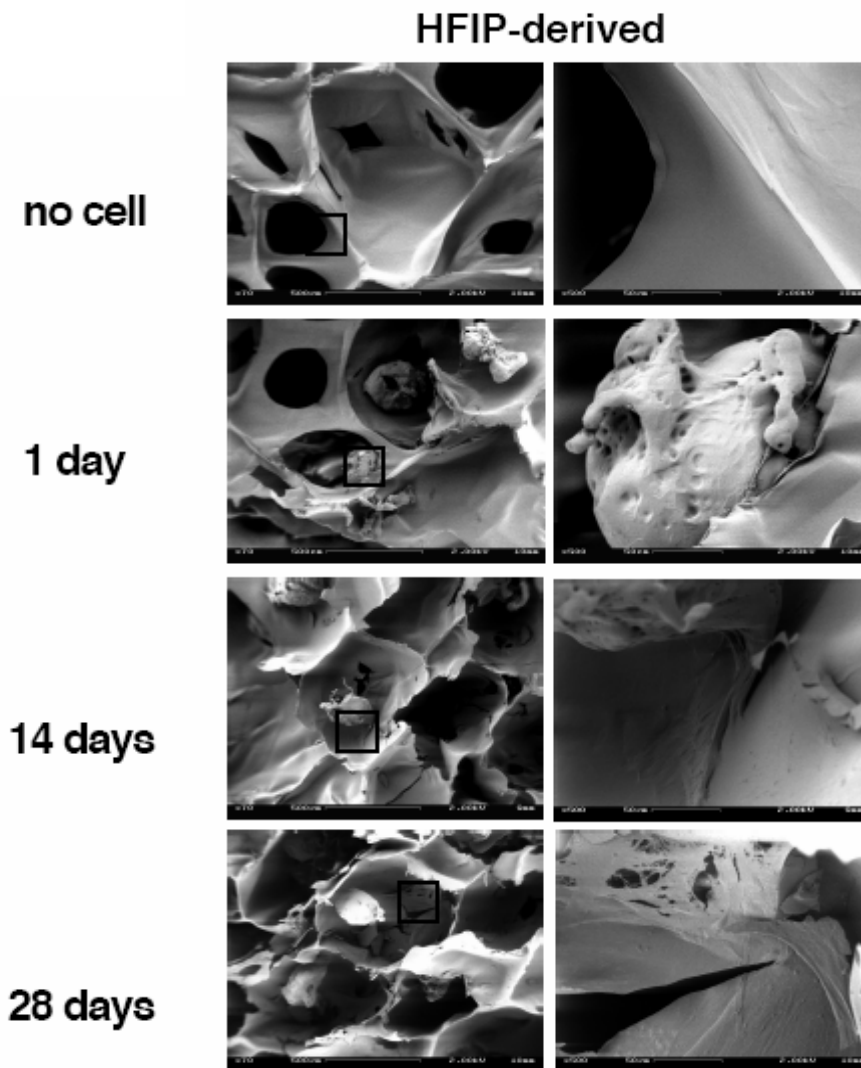


Figure 17: SEM of hMSCs in HFIP silk scaffolds. The images in the right column are magnified images of the boxed areas in the left column.

VII. Discussion

This study reports tissue-engineering of bone-like structures, investigating hMSCs (isolated from bone marrow), BMP-2 delivery, and silk fibroin scaffolds (in some cases decorated with RGD sequences). The *in vivo* DEXA results demonstrated that the defects with scaffolds loaded with BMP-2 and undifferentiated hMSCs (rat 73), the empty scaffolds (rat 74), and scaffolds with covalently bound RGD (rat 75) had bone area, content, and mineral density closest to their corresponding control values (Figure 16A-C). The highest density values were evident for rats 74 and 75 (Figure 15). This data does not correspond to the qualitative evaluation performed which showed rats 73 and 74 to have the most formation of new bone and bridging of the defect area (Figure 13). Since the qualitative evaluation is based on two independent observers, and is in fact qualitative, it is feasible to suspect inconsistencies within the analysts' evaluation. To resolve this uncertainty, more observers could be included in the evaluation. Despite this one contradiction, the remainder of the qualitative X-ray evaluation is corroborated by the DEXA.

The data gathered from this phase of the study conflicts with observations made from earlier results gathered by Hyeon Joo Kim and David Kaplan from Tufts University. The number of rats studied and their corresponding treatment group are in Table 17.

Table 17: Treatment groups for previous group of rats studied for critical size femoral defects

Group#	Treatment	Animals/group
1	Empty defect	4
2	Scaffolds with covalently bound RGD only	3
3	Defects with tissue-engineered scaffolds covalently bound to RGD (spinner flasks for 4 weeks)	4
4	Scaffolds with covalently bound RGD and undifferentiated hMSCs	2
5	BMP-2 loaded scaffolds	6
6	Scaffolds loaded with BMP-2 and tissue-engineered hMSCs	5
7	BMP-2 loaded scaffold and undifferentiated hMSCs (seeded the day before the surgery)	4

A qualitative evaluation was performed on this experimental group based on the same parameters defined in Table 14 (based on the bridging of the defect and the percentage of bone ingrowth). According to the qualitative scorings in the previous phase of the study, empty defects and defects with RGD covalently bound to scaffolds had minimal bone ingrowth and trace radiodense material over the 8 week time period (Figure 18). When undifferentiated hMSCs were added to the RGD scaffolds, there was no significant increase in new bone or bridging of the defect. There was, however, gradual bridging of the defect at both the cis and trans cortex when tissue engineered hMSCs were added (Figure 18A). At this time point, there was also new bone ingrowth that filled more than 50% of the defect (Figure 18B). The results also show that there is little difference in new bone and bridging of the defect between the tissue engineered scaffolds covalently bound to RGD and any of the BMP-2 loaded groups (Figure 18).

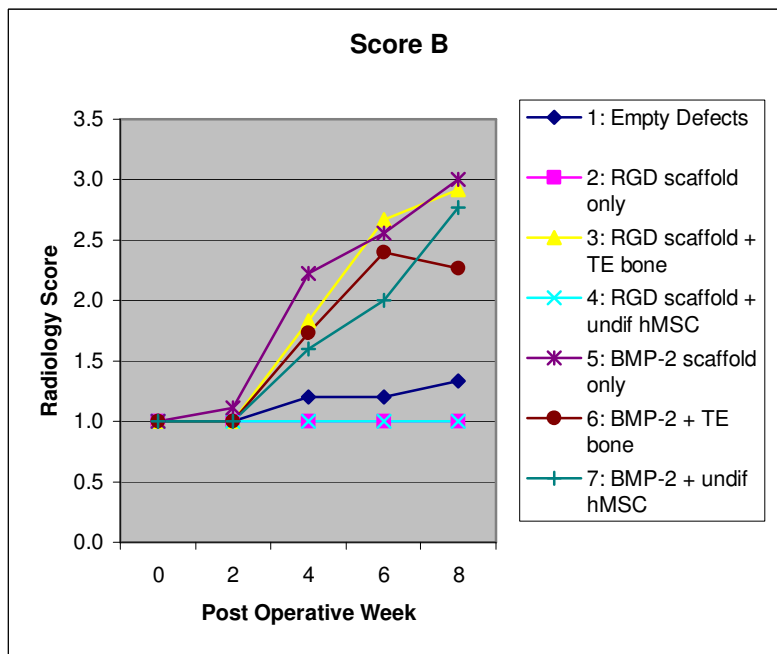
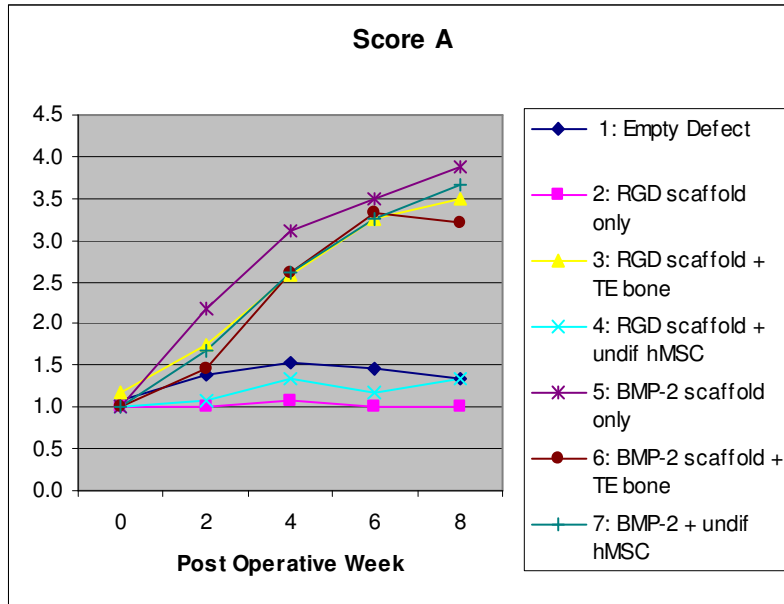


Figure 18: Qualitative analyses for bridging of the defect and percentage of bone ingrowth are shown in graphs A and B respectively. This was done for empty defects (Group 1), defects with scaffolds with covalently bound RGD (Group 2), defects with tissue engineered scaffolds with covalently bound RGD (Group 3), defects with scaffolds with covalently bound RGD and undifferentiated hMSCs (Group 4), defects with BMP-2 loaded scaffolds (Group 5), defects with tissue-engineered BMP-2 loaded scaffolds (Group 6) and defects with BMP-2 loaded scaffolds and undifferentiated hMSCs (Group 7). Data are represented as averages (n=2-6). Standard deviations ranged 0-0.98 (except for Group 4 where n=2). *adopted from Kaplan

DEXA scanning results for new bone area, mineral density, and content were also performed as was in the current experiment and did support the qualitative scoring obtained in Figure 18 (Figure 19). The defects that were loaded with BMP-2 (either alone or with hMSCs) and the scaffolds covalently bound RGD and tissue engineered hMSCs showed the highest bone ingrowth. These results show that effective osteogenesis occurred when hMSCs were tissue engineered *ex vivo* in spinner flasks for four weeks. In contrast, BMP-2 greatly enhanced healing of the defect and the effect induced by BMP-2 was independent of the presence of hMSCs.

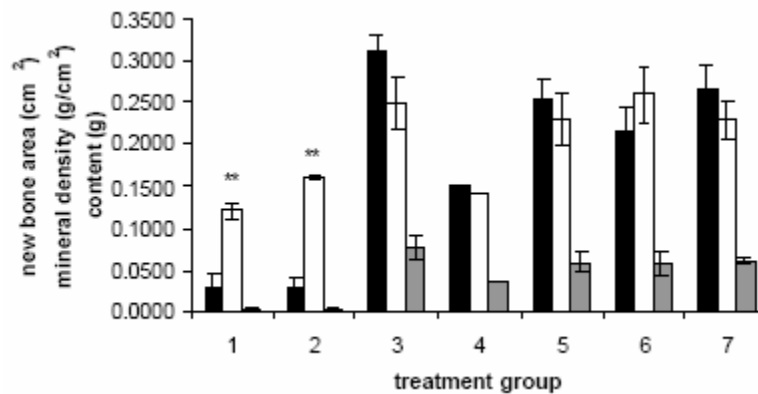


Figure 19: DEXA scanning of femoral defect with implants for new bone area (cm²) (black columns), mineral density (g/cm²) (white columns) and content (g) (gray columns) for empty defects (Group 1), defects with scaffolds with covalently bound RGD (Group 2), defects with scaffolds with covalently bound RGD and tissue engineered hMSCs (Group 3), defects with scaffolds with covalently bound RGD and undifferentiated hMSCs (Group 4), defects with BMP-2 loaded scaffolds (Group 5), defects with tissue-engineered BMP-2 loaded scaffolds (Group 6) and defects with BMP-2 loaded scaffolds and undifferentiated hMSCs (Group 7). Data are represented as averages \pm standard deviation (n=3-6). No standard deviation was included for Group 4, since n=2. *adopted from Kaplan

In the above group, the extent of osteogenesis were markedly higher, according to all measured parameters, for defects with RGD covalently bound to scaffolds with tissue engineered hMSCs and for all scaffolds loaded with BMP-2. This result is inconsistent with the current data collected. Although there was high bone ingrowth for BMP-2 loaded scaffolds with undifferentiated hMSCs, growth was also significant for empty defects (rat 74) and RGD scaffolds (rat 75) (Figure 15 & 16). These differences could be attributed to, at least in part, to the small groups that were used in this phase of the study (n=1, n=0, or n=2). Additionally, rat 76

did not show as significant healing as did rat 75, which demonstrates that there is great rat to rat variation considering they are both in treatment group 2.

In the qualitative evaluation and the DEXA scanning, the empty defect resulted in the most new bone growth and the most bridging (Figure 13) and area, content, and density values similar to the control (Figure 16). It is evident from Figure 14E that the empty defect induced the most new bone and obscured most of the cut cortices, although there were still cut edges visible. This indicates that osteoconductivity (presence of the scaffold) was sufficient to provide healing. The progression and extent of osteogenesis for silk scaffolds has been recognized in biomedical application, however it has been with the incorporation of growth factors and/or stem cells (Meinel *et al.*, 2004; Sofia *et al.*, 2000).

Tissue engineering of autologous bone using hMSCs are an obvious source of cells as long as they are seeded onto an appropriate substrate. They have the capability to proliferate in an undifferentiated state with the appropriate signaling factors. Additionally, they can be easily isolated and it has been proposed that the osteogenic pathway is their default lineage (Meinel *et al.*, 2004; Banfi *et al.*, 2002). It has been demonstrated that the addition of hMSCs to silk/RGD constructs are effective only if tissue engineered *ex vivo*. RGD is capable of binding the intracellular cytoskeleton of the hMSCs to the matrix, however it is not osteoinductive. This is true with the previous results. The RGD constructs alone did induce bone formation, however. This is attributed to rat to rat variation rather than to the effectiveness of the scaffold itself.

The effect of BMP-2 on bone formation was dominated by any effect of hMSCs (Figures 18 & 19). This proves that the addition of BMP-2 was enough to induce osteoinductivity. The current experiment could not generate this conclusion because only one specimen had BMP-2

incorporated onto the scaffold. However, the data suggested that the formation of new bone was significant for the rat with BMP-2 (rat 73) (Figure 15 & 16).

In regards to the treatment group with the RGD scaffold only, the previous data are in accordance with the current results for the qualitative evaluations. However, the current DEXA data (Figure 15) shows that there were high bone mineral density, content, and area for rat 75 and high density for rat 76 which are not evident in Figure 19. It is evident that the data generated in this experiment did not mirror that of the previous one. As mentioned, possibilities for these differences may stem from smaller sample sizes and great rat to rat variation. It can also be speculated that the fabrication method of the scaffolds resulted in significant matrix heterogeneity. This is likely due to the evaporation of the solvent (Nazarov *et al.*, 2003). As a result there can also be scaffold to scaffold variation, which will ultimately change the healing process and new bone formation independent of the growth factors or stem cells. Research has suggested that the silk scaffold geometry and morphology predetermines the geometry of the new engineered bone. It can be speculated that the morphology of the certain scaffolds imparted diffusional limitations which restricted the formation of compact and contiguous bone.

Another study conducted at Tufts University by Kim *et al.* described a new process to form silk scaffolds. This aqueous-derived scaffold avoided the use of organic solvents and resulted in a more uniform morphology compared to that of the HFIP-derived silk scaffolds used in this experiment. The more homogenous a scaffold is throughout will provide improved mechanical properties of the matrix. This is because stress is concentrated at pore interfaces and the lack of uniformity typically causes deformation at lower stresses (Harris *et al.*, 1998).

In summary, tissue engineered bone was created for defects that were empty and defects with scaffolds loaded with BMP-2. This was corroborated with DEXA scanning. DEXA,

however, also demonstrated that new bone was formed for the defects with silk/RGD constructs only (rat 75 but not rat 76). This data differs from the results gathered from the previous group that was analyzed. Such differences could be explained by the small experimental groups, rat to rat variation, and scaffold to scaffold variation that comes from the fabrication method.

VIII. Conclusions

Porous, three-dimensional silk fibroin matrices were prepared from the addition of HFIP and methanol and fabricated by a method of salt leaching. Combinations of RGD +/- hMSCs or BMP-2 +/- hMSCs were added to the silk scaffolds to determine which combination induced tissue engineered bone. According to qualitative analysis, the *in vivo* study demonstrated that the defects with the empty scaffolds (rat 74) and scaffolds loaded with BMP-2 and undifferentiated hMSCs (rat 73) induced formation of new bone and bridged the defect over an eight week time period. The DEXA analysis showed similar results except the defects with silk/RGD constructs only (rat 75) had similar bone ingrowth to rats 73 and 74.

The distinguishing features of silk fibroin made it an appealing scaffold biomaterial for the demanding and unique environment of bone. The protein provides mechanical integrity that match the repair site and also allows for control of the properties through various processing methods. Additionally, silk is biocompatible, resorbable, has a diverse surface chemistry, is highly organized, and has a beneficial overall tailorability that is unattainable with other biomaterials used in today's technology.

Although there are some contradictory results within the data, when the mechanical features of silk are considered in addition to biocompatibility, biodegradability, and versatility in chemistry, these silk biomaterials offer new and important options in designing three-dimensional matrices. Furthermore, when coupled with the processing and fabrication options available for silks, the biomaterial can be improved and generate a range of materials and properties.

IX. Future Recommendations

Further analysis is needed to confirm the osteogenesis of the scaffold: 1) Investigate tissue reaction to the silk constructs by histology tests (including necrosis, inflammation, giant cells, macrophages, and scarring); 2) Micro-computer tomography; 3) Measure degradation rate of the product as well as mechanical properties (Young's modulus and compression).

In order to better evaluate osseointegration of the tissue engineered construct, a 3-D evaluation technique could be employed called micro-computed tomography. This non-destructive method could characterize the regeneration of bone tissue at the micron scale. Such a technique would also help to further understand the process of tissue engineered bone ingrowth. This, in turn, could potentially optimize scaffold design since there is still a great deal unknown about structural and transport properties during tissue ingrowth. This type of analysis could complement the type of analysis techniques performed and answer questions that would otherwise be unanswered. For example, the technique could establish if the bone within the scaffold is interacting with the native bone and determine the direction of mineralization. This is important because with the 2-D analysis that was conducted in the current experiment, it is difficult to determine whether the observed growth is from the host femur bone or rather outgrowth for the silk construct.

During experimental process, there were a few points observed that may be conducted slightly different during future experiments in order to improve the outcome of the results. When the X-rays were taken of the rats' femurs, they were not all taken in the same position. This could have obscured the qualitative analysis in that the new bone growth was not seen clearly. When future experiments are conducted, they might try positioning all of the legs in the exact same angle, possibly through building an apparatus to hold the femur in place.

Additionally, the constructs should be enhanced based on the knowledge obtained from the experiment to more fully meet the structural, mechanical, and physiochemical properties of bone scaffolds.

References

- Agrawal, C., Bay, R. Biodegradable polymeric scaffolds for musculoskeletal tissue engineering. *Journal of Biomedical Materials Research* 55 (2000) 141-150.
- Altman, G., Diaz, F., Jakuba, C., Calabro, T., Horan, R., Chen, J., Lu, H., Richmond, J., Kaplan, D. Silk-Based Biomaterials. *Biomaterials* 24 (2003) 401-416.
- Arrington ED, Smith WJ, Chambers HG, Bucknell AL, Davino NA. Complications of iliac crest bone graft harvesting. *Clinical Orthopedics*.329; (1996) 300-309.
- Asakuras, T., Kaplan, D. Silk production and processing. Arutzen CJ, editor. Encyclopedia of agricultural science. New York: Academic; 1994. Vol 4 p. 1-11.
- Banfi, A., Bianchi, G., Notaro, R., Luzzatto, L., Cancedda, R., Quarto, R. Replicative aging and gene; Expression in long-term cultures of human bone marrow stromal cells. *Tissue Engineering* 8 (2002) 901-910
- Barry, F., Murphy, J. Mesenchymal stem cells: clinical applications and biological characterization. *The International Journal of Biochemistry & Cell Biology* 36 (2004) 568-584.
- Bellows, C., Aubin J. Determination of numbers of osteoprogenetors present in isolated fetal rat calvaria cells *in vitro*. *Developmental Biology* 133 (1989) 8-13.
- Bini, E., Knight, D., Kaplan, D. Mapping domain structures in silks from insects and spiders related to protein assembly. *J. Mol. Bio.* 335 (2004) 27-40.
- Bohner, M. Calcium orthophosphates in medicine: from ceramics to calcium phosphate cements. *Injury, International Journal of the Care of the Injured* 31 (2000) SD37-47.

- Bucholz, R., Carlton, A., Holmes, R. Hydroxyapatite and tri-calcium phosphate bone graft substitutes. *Orthop Clin North America* 18 (1987) 323-334.
- Craig, C., Riekkel, C. Comparative architecture of silks, fibrous proteins and their encoding genes in insects and spiders. *Comparative Biochemistry and Physiology Part B* 133 (2002) 493-507.
- Fang, J., Zhu, Y., Smiley, E., Bonadio, J., Rouleau, P., Goldstein, S., McCauley, L., Davidson, B., Roessler, B. *Proc. Natl. Acad. Sci.* 93 (1996) 5753-5758.
- Gauthier, O., Bouler, J., Weiss, P., Bosco, J., Daculsi, Guy, Aguado, E. Kinetic study of bone ingrowth and ceramic resorption associated with the implantation of different injectable calcium-phosphate bone substitutes. *Biomed Mater Res* 47 (1999) 28-35.
- Grabarek, Z., Gergely, J. Zero-length cross-linking procedure with the use of active esters. *Anal Biochem* 185 (1990) 131-135.
- Harris, L., Kim, B., Mooney, D. Open pore biodegradable matrices formed with gas foaming. *J Biomed Mat Res* 42 (1998) 396-402
- Hockin, H., Xu, K., Simon, C. Fast setting calcium phosphate-chitosan scaffold: mechanical properties and biocompatibility. *Biomaterials* 26 (2005) 1337-1348.
- Jarcho, M. Calcium phosphate ceramics as hard tissue prosthetics. *Clin Orthop Rel Res* 157 (1981) 259-278.
- Kaplan, D. Fibrous proteins-silk as a model system. *Polymer Degradation and Stability* 59 (1998) 25-32.
- Kim, U., Park, J., Kim, H., Wada, M., Kaplan, D. Three-dimensional aqueous-deprived biomaterial scaffolds from silk fibroin. *Biomaterials* (2004) 1-10

- Kikuchi, M., Suetsugu, Y., Tanaka, J. Preparation and mechanical properties of calcium phosphate/copoly-L-lactide composites. *Journal of Materials Science* 8 (1997) 361-364.
- Laurencin, C., Ambrosio A., Borden, M., Cooper Jr., J. Tissue engineering: orthopedic applications. *Annual Review Biomed Eng* 1 (1999) 19-46.
- Mauney, J., Sjostrom, S., Blumberg, J., Horan, R., O'Leary, J., Vunjak-Novakovic, G., Volloch, V., Kaplan, D. Mechanical stimulation promotes osteogenic differentiation of human bone marrow stromal cells on 3-D partially demineralized bone scaffolds *in vitro*. *Calcified Tissue International* 74 (2003) 458-468.
- Meinel, L., Karageorgiou, V., Hofmann, S., Fajardo, F., Snyder, B., Li, C., Zichner, L., Langer, R., Vunjak-Novakovic, G., Kaplan, D. Engineering bone-like tissue *in vitro* using human bone marrow stem cells and silk scaffolds.
- Meinel, L., Hoffman, S., Karageorgiou, V. Kirker-Head, C., McCool, J., Gronowicz, G., Zichner, L., Langer, R., Kaplan, D., D. The inflammatory response to silk films *in vitro* and *in vivo*. *Biomaterials* 26 (2004) 147-155.
- Petite, H., Viateau, V., Bensaid, W., Meunier, A., Pollak, C., Bourguignon, M., Oudina, K., Sedel, L., Guillemain, G. Tissue-engineered bone regeneration. *Nature Biotechnology* 18 (2000) 959-963.
- Rey, C. Calcium phosphate biomaterials and bone mineral: Differences in composition, structures and properties. *Biomaterials* 11 (1990) 13-15.
- Rho, J., Kuhn-Spearing, L, Zioupos, P. Mechanical properties and the hierarchial structure of bone. *Medical Engineering & Physics* 20 (2003) 92-102.
- Saito, N. New synthetic biodegradable polymers as BMP carriers for bone tissue engineering. *Biomaterials* 24 (2003) 2287-2293.

- Scheibel, T. Spider silks: recombinant synthesis, assembly, spinning, and engineering of synthetic proteins. *Microbial Cell Factories* 3 (2004) 3-14.
- Sofia, S., McCarthy, M., Gronowicz, G., Kaplan, D. Functionalized silk-based biomaterials for bone formation. *Journal of Biomedical Materials Research* 54 (2000) 139-148.
- Taylor, M., Daniels, A., Andriano, K., Heller, J. Six bioabsorbable polymers: in vitro acute toxicity of accumulated degradation products. *Biomaterials* 2 (1994) 151-157.
- Xu, H., Simon, C. Fast setting calcium phosphate-chitosan scaffold: mechanical properties and biocompatibility. *Biomaterials* 26 (2004) 1337-1348.
- Valluzzi, R., Winkler, S., Wilson, D., Kaplan, D. Silk: molecular organization and control of assembly. *Phil. Trans. R. Soc. Lond.* 357 (2002) 165-167.
- Yaszemski, M., Payne, R., Hayes, W., Langer, Mikos, A. Evolution of bone transplantation: molecular, cellular and tissue strategies to engineer human bone. *Biomaterials* 17 (1996) 175-185.
- Zhao, C., Asakura, T. Structure of silk studied with NMR. *Progress of Nuclear Magnetic Resonance Spectroscopy* 39 (2002) 301-352.
- Zhao, C., Yao, J., Masuda, H., Kishore, R., Asakura, T. Structural characterization and artificial fiber formation of *Bombyx mori* silk fibroin in Hexafluoro-Iso-Propanol solvent system. *Biopolymers* 69 (2003) 253-259.

Appendices

Appendix A

Methods of Analysis

Dual-Energy X-ray Absorptiometry

In order to measure bone density, scientists often look to an enhanced form of x-ray technology called dual-energy x-ray absorptiometry (DEXA). DEXA has become the standard for measuring bone mineral density (BMD) (American College of Radiology & Radiological Society of North America, 2003). The procedure is a fast and painless method for measuring if bone loss or formation is occurring.

The DEXA procedure takes between 10 and 30 minutes to perform. The device transfers a visible beam of low-density x-rays through the bone by means of two energy streams (American College of Radiology & Radiological Society of North America, 2003). It relies on two distinct energy peaks: one peak is absorbed mainly by soft tissue and the other by bone. The soft tissue amount can be subtracted from the total, and what remains is a patient's bone mineral density (American College of Radiology & Radiological Society of North America, 2003). The data then is displayed on a computer screen in order to make a diagnosis.

Computed Tomography (CT) Scan

A micro Computed Tomography (CT) scan, particularly the GE eXplore RS model, is also utilized in order to measure the success of biomaterials. “It is an ideal instrument for biomedical research laboratories to non-destructively acquire 3-D images of both *in vivo* and *in vitro* specimens” (GE Healthcare, 2004). The GE eXplore RS is used particularly for small laboratory animals such as rats or mice. It is able to capture whole body images at 45 or 90 μm

and *in vitro* specimens at 27 μm (GE Healthcare, 2004). GE eXplore RS CT scans have Conebeam CT technology, enabling the total volume of a sample to be imaged in one rotation, instead of having to measure slice by slice.

Radiographs

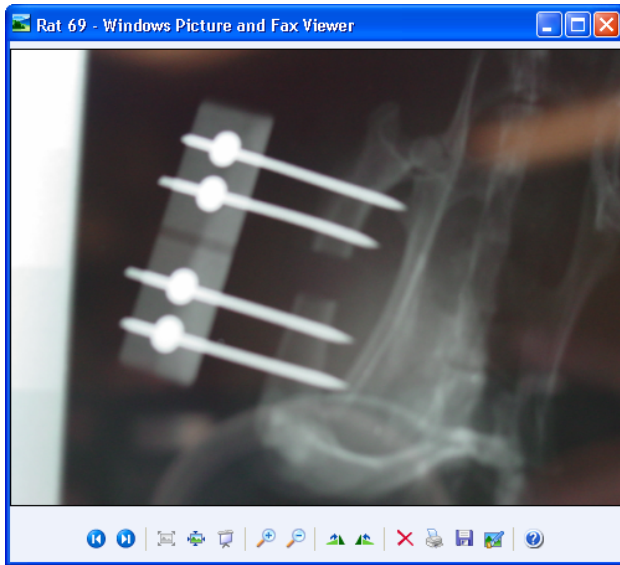
This technique is used to follow healing after bone defects are made. Usually the wound is followed radiographically every 2 or 4 weeks. Such post-operative procedures provide a means to qualitatively monitor the level of bone regeneration and implant resorption. However, there are methods in which the radiographs can be digitized to present quantitative data.

Appendix B

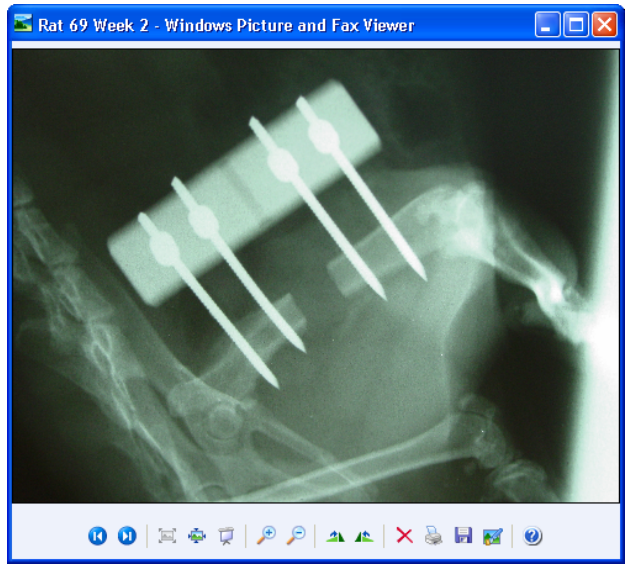
Radiographs

Rat #69:

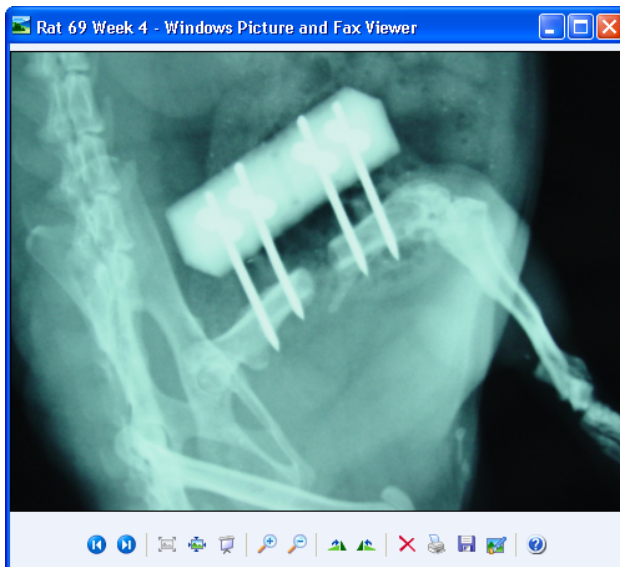
Week 0



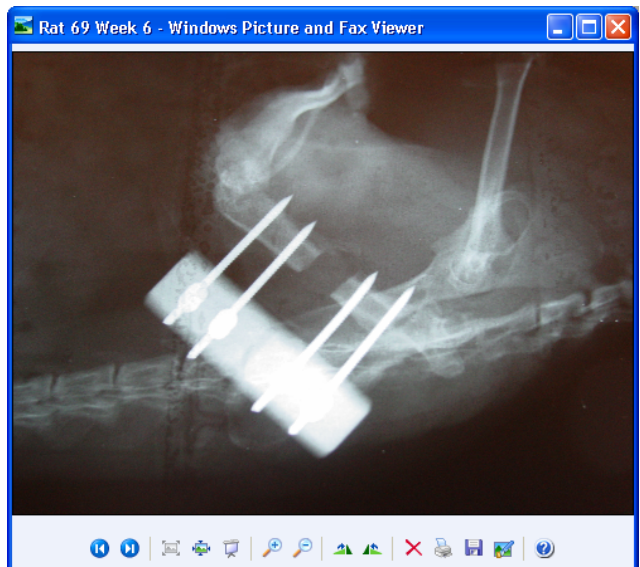
Week 2



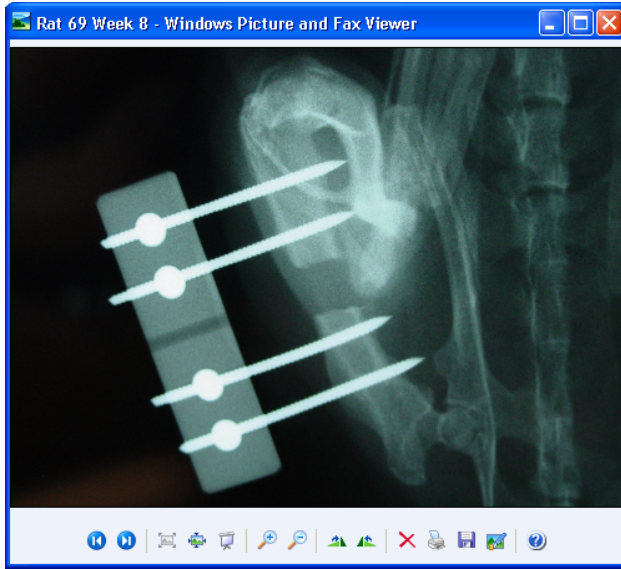
Week 4



Week 6

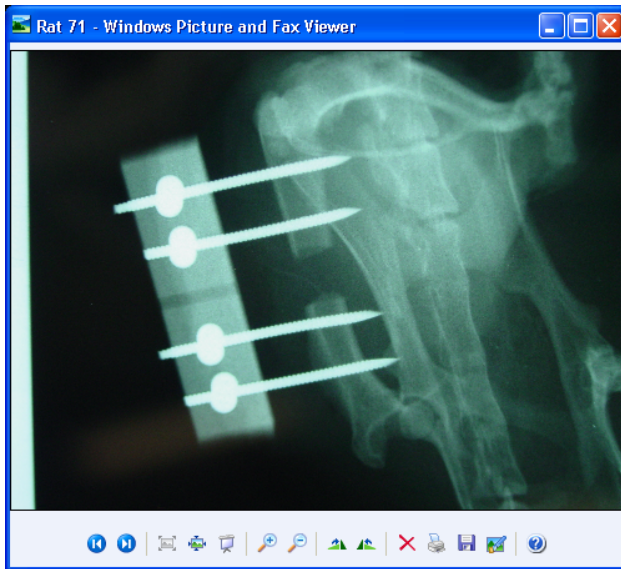


Week 8

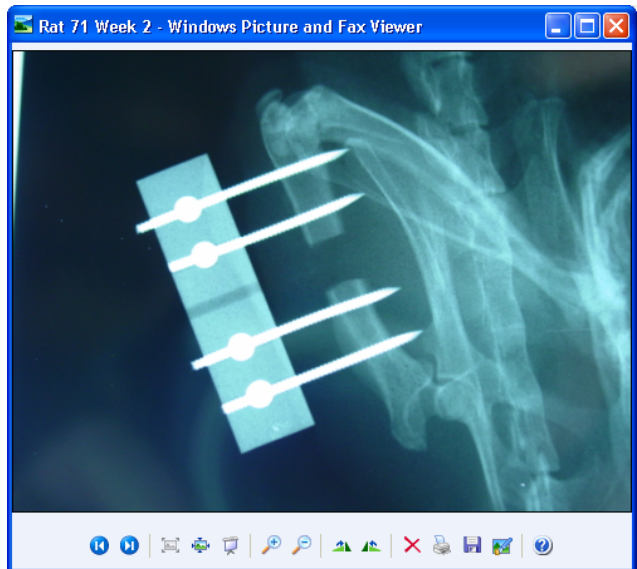


Rat #71:

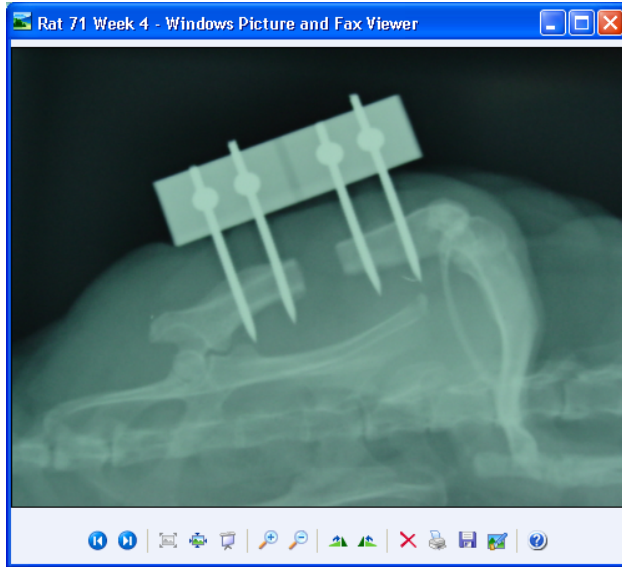
Week 0



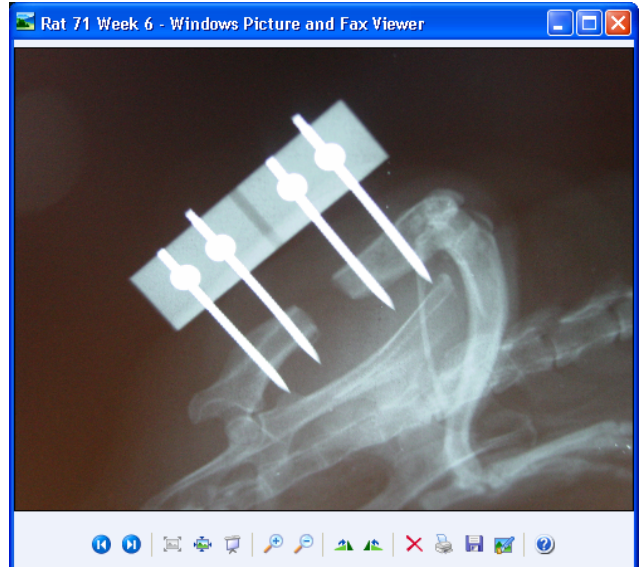
Week 2



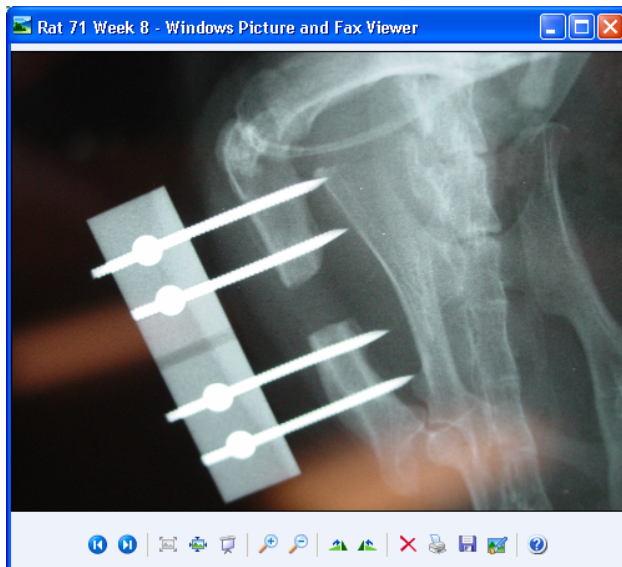
Week 4



Week 6

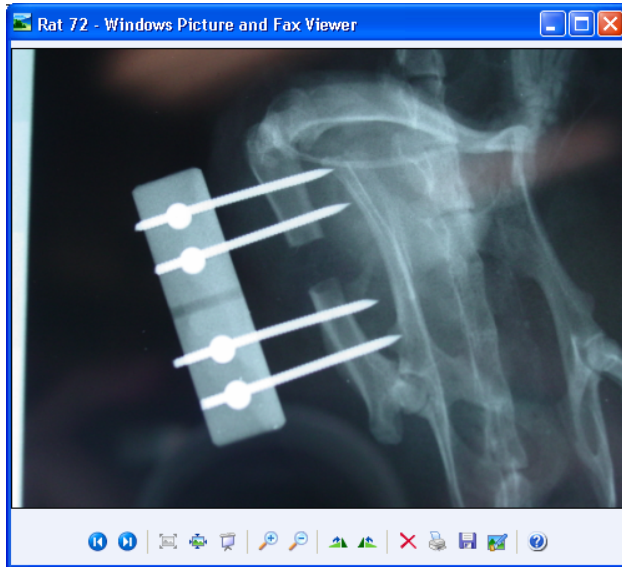


Week 8

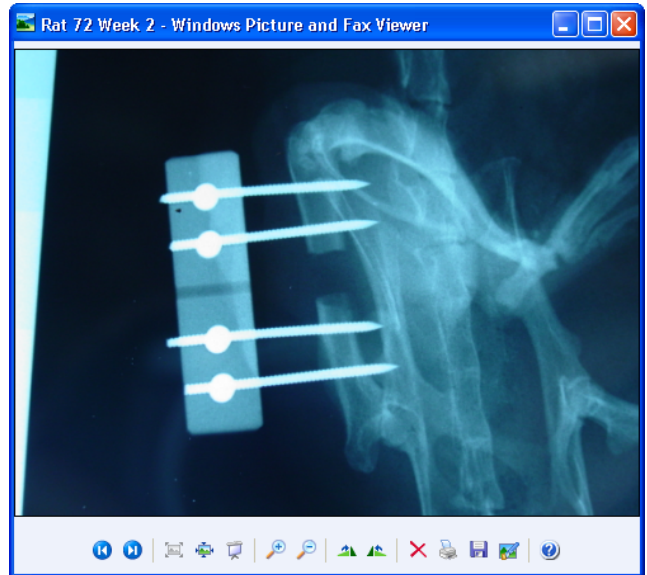


Rat #72:

Week 0

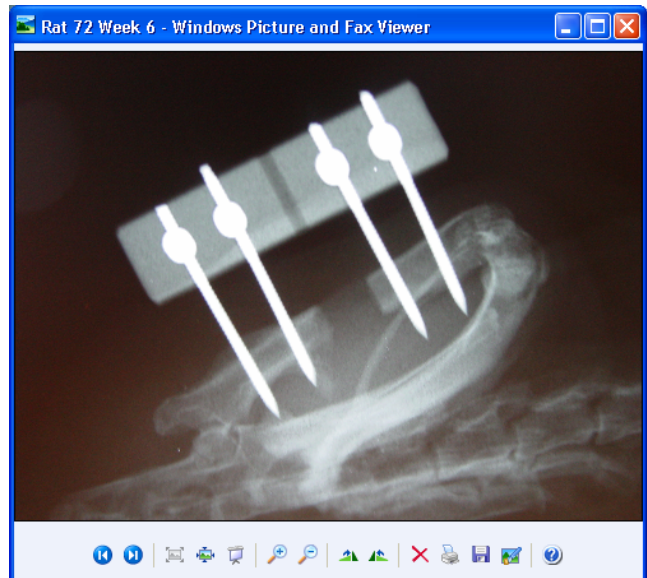


Week 2

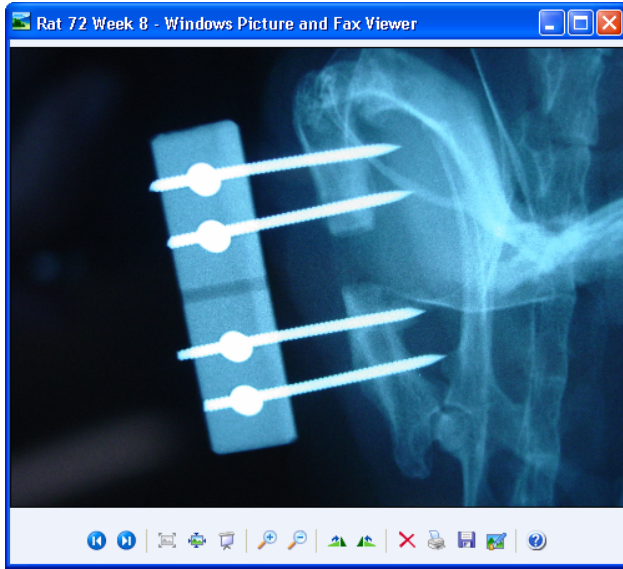


Week 4

Week 6

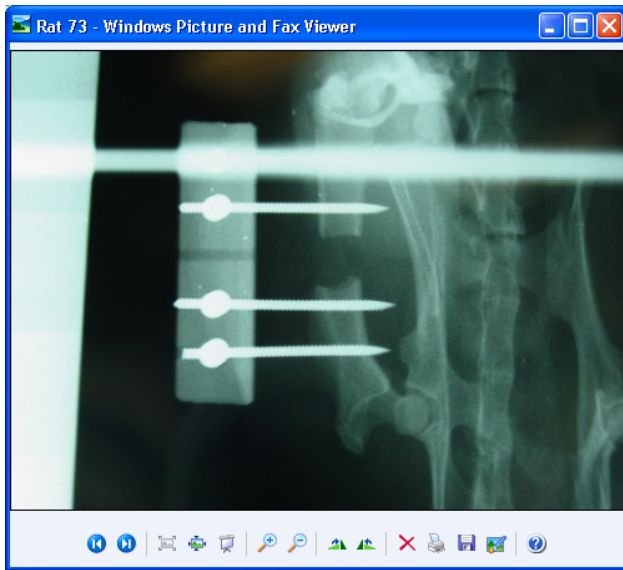


Week 8

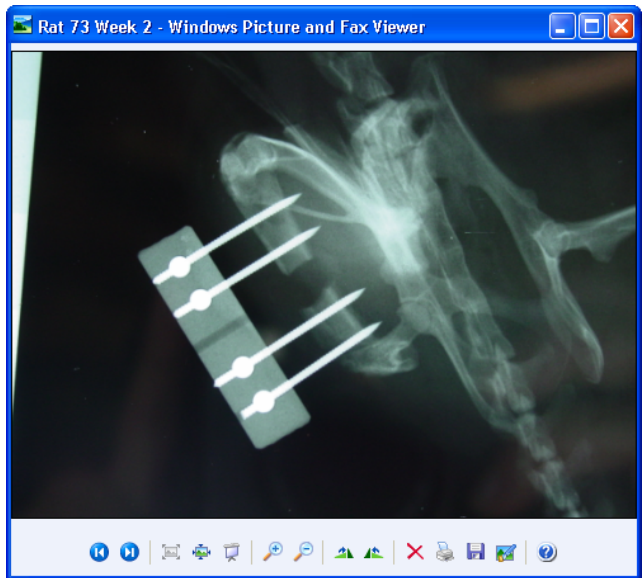


Rat #73:

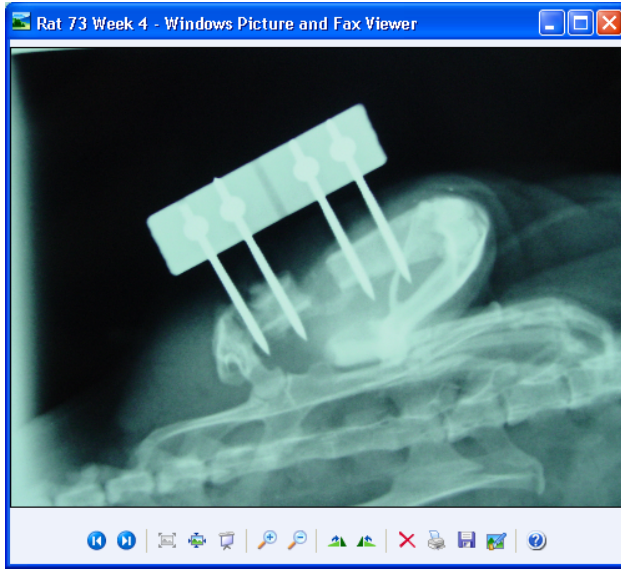
Week 0



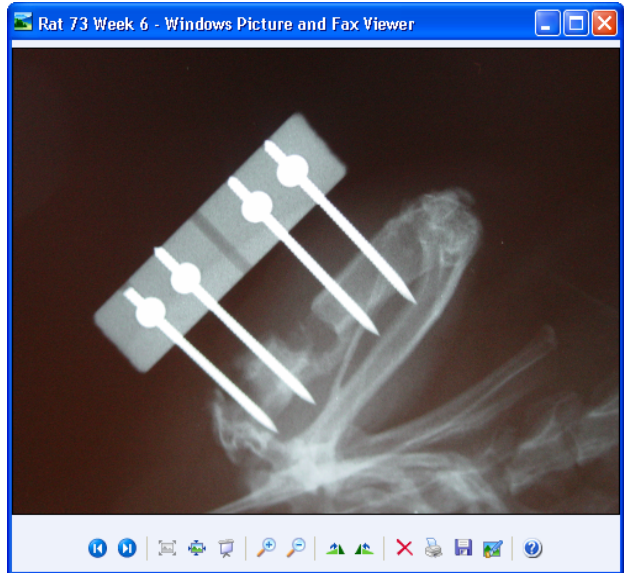
Week 2



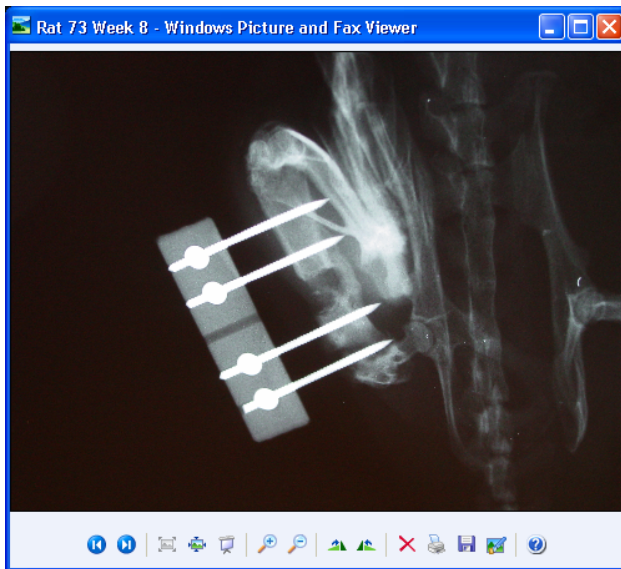
Week 4



Week 6

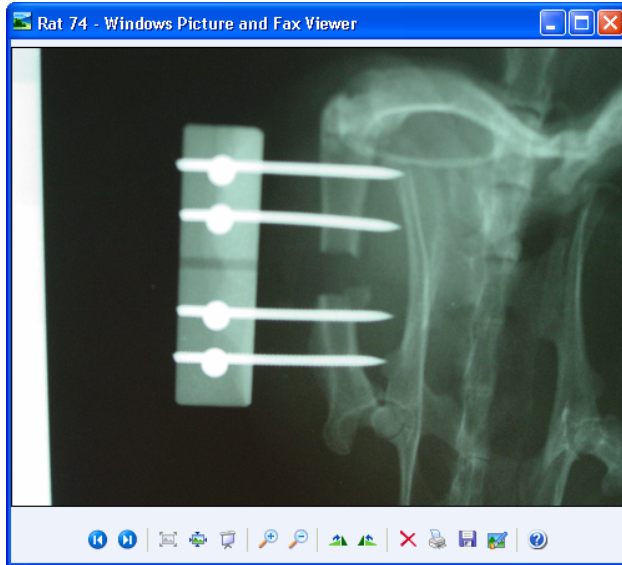


Week 8

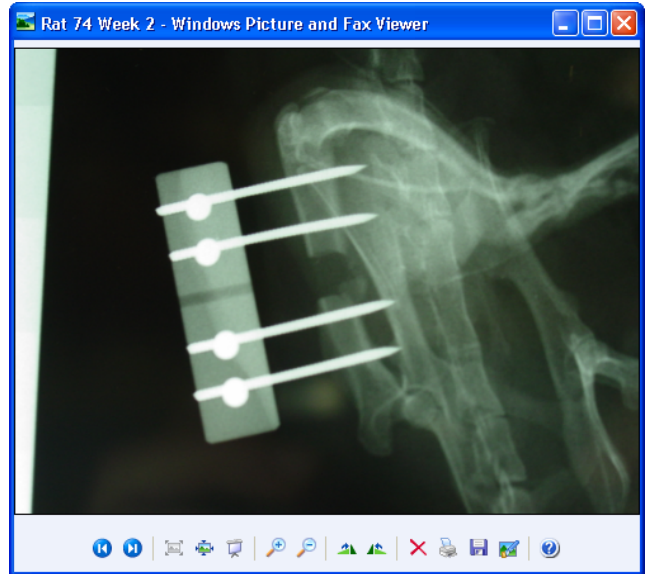


Rat #74:

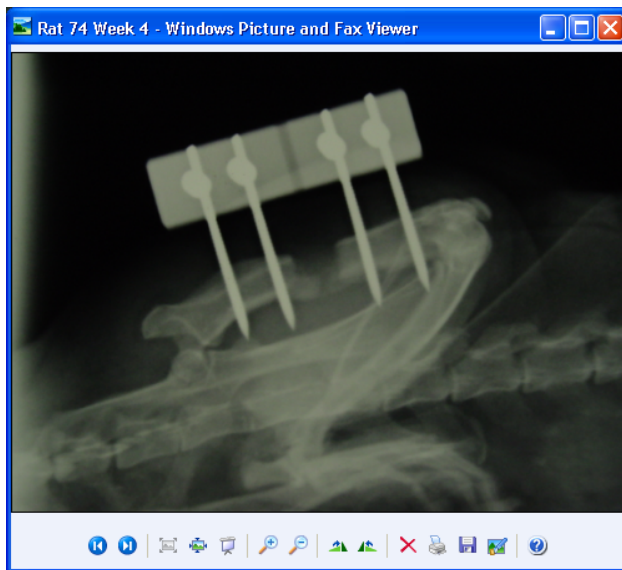
Week 0



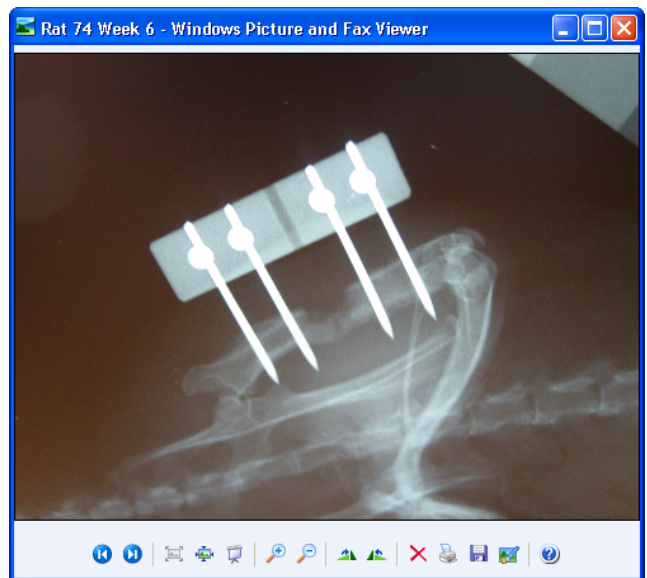
Week 2



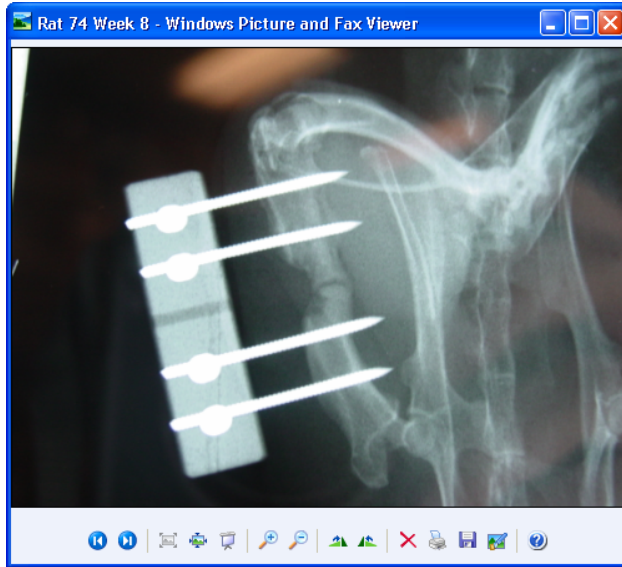
Week 4



Week 6

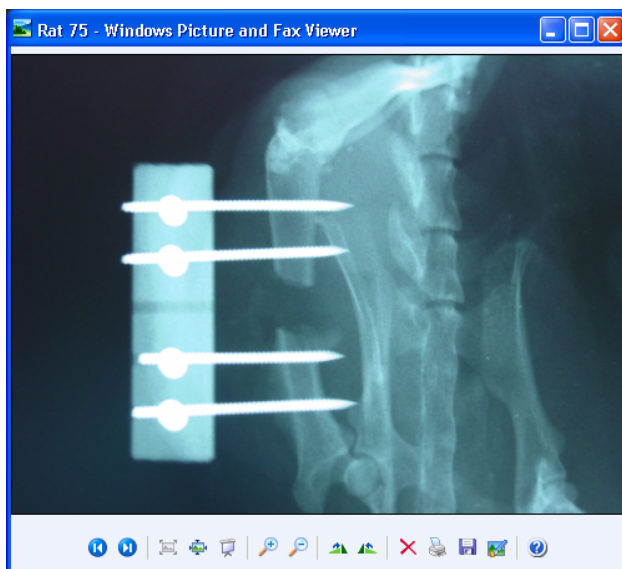


Week 8

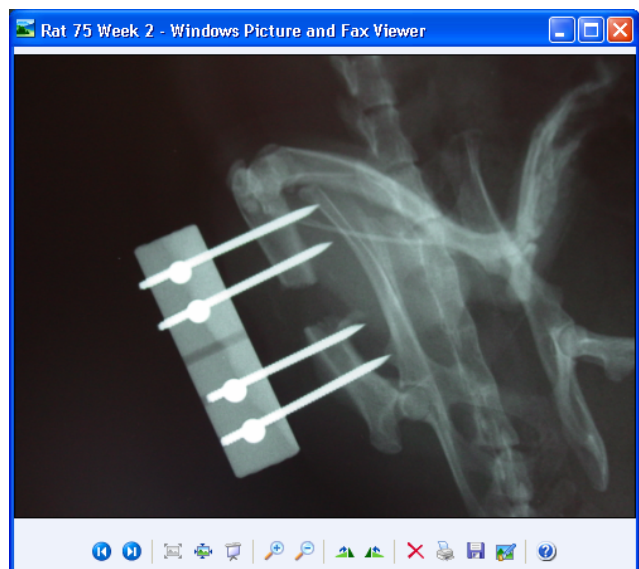


Rat #75:

Week 0



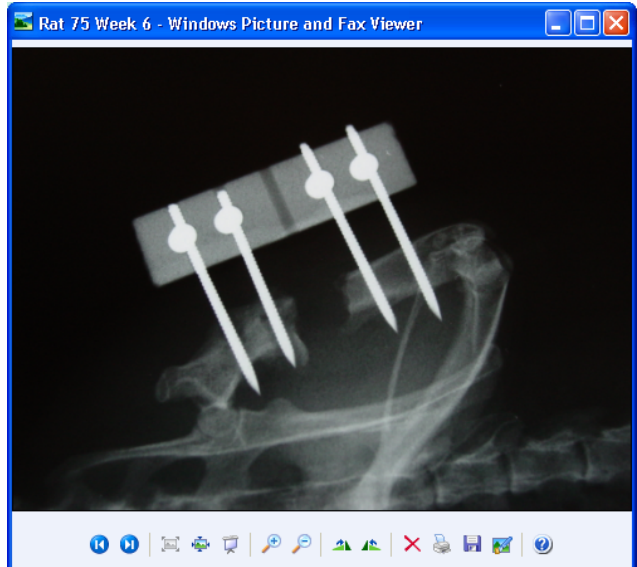
Week 2



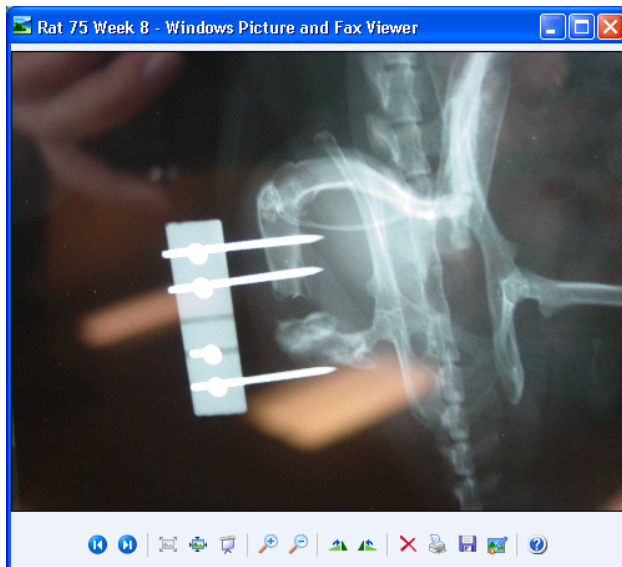
Week 4



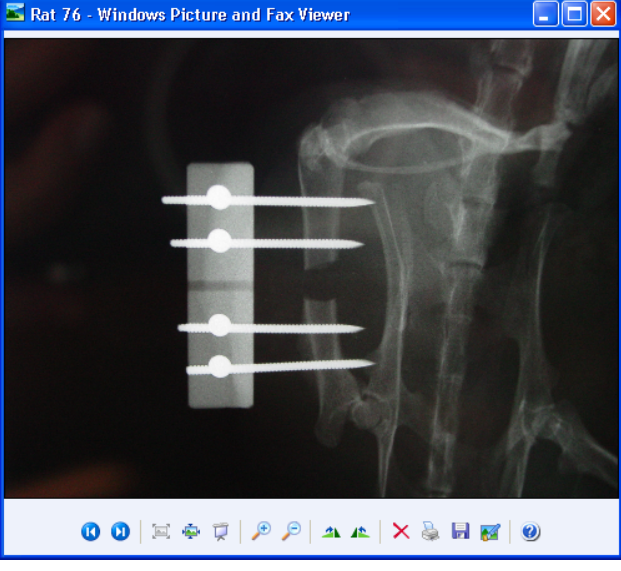
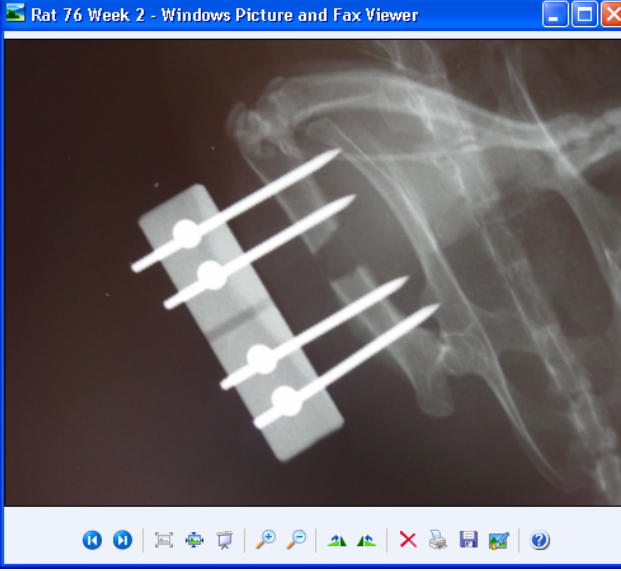
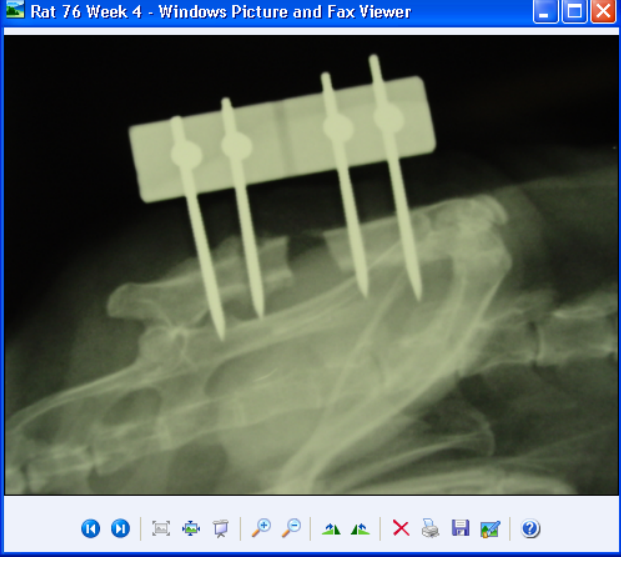
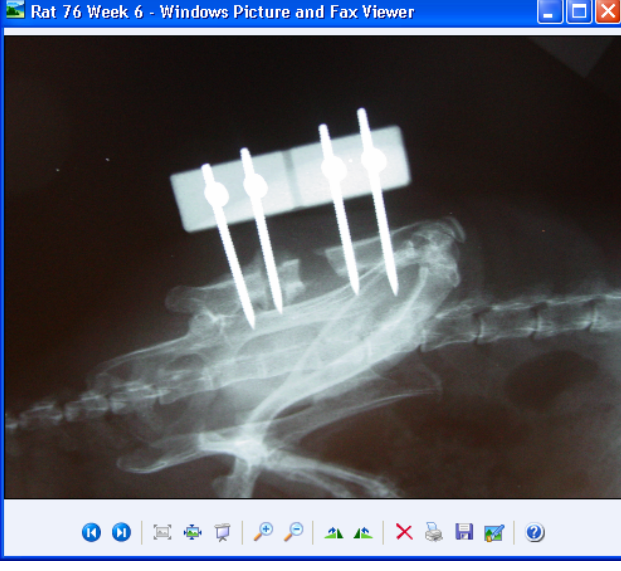
Week 6



Week 8



Rat #76:

Week 0	Week 2
 <p>Rat 76 - Windows Picture and Fax Viewer</p> <p>This X-ray shows a rat's spine with a vertical plate and four screws. The plate is positioned on the left side of the spine, and the screws are inserted into the vertebral bodies. The window title is "Rat 76 - Windows Picture and Fax Viewer".</p>	 <p>Rat 76 Week 2 - Windows Picture and Fax Viewer</p> <p>This X-ray shows the rat's spine at Week 2. The vertical plate and four screws are still present, but they appear slightly tilted and less aligned with the spine compared to Week 0. The window title is "Rat 76 Week 2 - Windows Picture and Fax Viewer".</p>
Week 4	Week 6
 <p>Rat 76 Week 4 - Windows Picture and Fax Viewer</p> <p>This X-ray shows the rat's spine at Week 4. The vertical plate and four screws are still present, but they appear significantly tilted and less aligned with the spine compared to Week 0. The window title is "Rat 76 Week 4 - Windows Picture and Fax Viewer".</p>	 <p>Rat 76 Week 6 - Windows Picture and Fax Viewer</p> <p>This X-ray shows the rat's spine at Week 6. The vertical plate and four screws are still present, but they appear significantly tilted and less aligned with the spine compared to Week 0. The window title is "Rat 76 Week 6 - Windows Picture and Fax Viewer".</p>

Appendix C

DEXA Scanning of Defected Area

Rat #69:

Defect Area

Region	Area (cm²)	Bone mineral content (g)	Bone mineral density (g/cm²)
Global	0.2143	0.0596	0.2780
R1	0.0047	0.005	0.1056
R2	0.0056	0.0006	0.1138
R3	0.0000	0.0000	0.0000

Rat #71:

Defect Area

Region	Area (cm²)	Bone mineral content (g)	Bone mineral density (g/cm²)
Global	0.1565	0.0484	0.3090
R1	0.0000	0.0000	0.0000
R2	0.0000	0.0000	0.0000
R3	0.0000	0.0000	0.0000

Rat #72:

Defect Area

Region	Area (cm²)	Bone mineral content (g)	Bone mineral density (g/cm²)
Global	0.1593	0.0431	0.2704
R1	0.0093	0.0013	0.1355
R2	0.0093	0.0013	0.1355
R3	0.0000	0.0000	0.0000

Rat #73:**Defect Area**

Region	Area (cm²)	Bone mineral content (g)	Bone mineral density (g/cm²)
Global	0.4081	0.1137	0.2786
R1	0.1360	0.0224	0.1647
R2	0.1854	0.0298	0.1608
R3	0.0811	0.0099	0.1222

Rat #74:**Defect Area**

Region	Area (cm²)	Bone mineral content (g)	Bone mineral density (g/cm²)
Global	0.3317	0.0819	0.2470
R1	0.1258	0.0250	0.1985
R2	0.1277	0.0252	0.1970
R3	0.0457	0.0084	0.1834

Rat #75:**Defect Area**

Region	Area (cm²)	Bone mineral content (g)	Bone mineral density (g/cm²)
Global	0.3942	0.1187	0.3012
R1	0.0801	0.0189	0.2363
R2	0.1323	0.0296	0.2236
R3	0.0112	0.0020	0.1765

Rat #76:**Defect Area**

Region	Area (cm²)	Bone mineral content (g)	Bone mineral density (g/cm²)
Global	0.2357	0.0567	0.2403
R1	0.0307	0.0055	0.1782
R2	0.0345	0.0058	0.0169
R3	0.0000	0.0000	0.0000

Appendix D

DEXA Scanning of Control Area

Rat #69:

Control Area

Region	Area (cm²)	Bone mineral content (g)	Bone mineral density (g/cm²)
Global	0.4137	0.0913	0.2206
R1	0.2069	0.0440	0.2128
R2	0.2078	0.0446	0.2144
R3	0.2059	0.0436	0.2117

Rat #71:

Control Area

Region	Area (cm²)	Bone mineral content (g)	Bone mineral density (g/cm²)
Global	0.3839	0.0811	0.2138
R1	0.1901	0.0406	0.2137
R2	0.1892	0.0394	0.2085
R3	0.1901	0.0414	0.2177

Rat #72:

Control Area

Region	Area (cm²)	Bone mineral content (g)	Bone mineral density (g/cm²)
Global	0.4072	0.0886	0.2177
R1	0.1975	0.0427	0.2159
R2	0.1966	0.0414	0.2105
R3	0.1975	0.0431	0.2182

Rat #73:

Control Area

Region	Area (cm²)	Bone mineral content (g)	Bone mineral density (g/cm²)
Global	0.4147	0.0870	0.2099
R1	0.2003	0.0397	0.1979
R2	0.2013	0.0397	0.1973
R3	0.2013	0.0400	0.1990

Rat #74:

Control Area

Region	Area (cm²)	Bone mineral content (g)	Bone mineral density (g/cm²)
Global	0.3355	0.0798	0.2378
R1	0.1696	0.0396	0.2337
R2	0.1705	0.0412	0.2416
R3	0.1668	0.0386	0.2316

Rat #75:

Control Area

Region	Area (cm²)	Bone mineral content (g)	Bone mineral density (g/cm²)
Global	0.5106	0.1293	0.2532
R1	0.1659	0.0409	0.2467
R2	0.1649	0.0406	0.2460
R3	0.1668	0.0411	0.2464

Rat #76:

Control Area

Region	Area (cm²)	Bone mineral content (g)	Bone mineral density (g/cm²)
Global	0.4137	0.0714	0.1727
R1	0.1985	0.0334	0.1685
R2	0.1966	0.0332	0.1689
R3	0.2050	0.0346	0.1688